NAVAL POSTGRADUATE SCHOOL

MONTEREY, CALIFORNIA

THESIS

SHORT-RANGE ACOUSTIC PROPAGATION USING MOBILE TRANSMITTERS UNDER ARCTIC ICE COVER

by

Liam J. Doyle

September 2017

Thesis Advisor: John Joseph
Co-Advisor: D. Benjamin Reeder

THIS PAGE INTENTIONALLY LEFT BLANK

REPORT DOCUMENTATION PAGE			Form Approved OMB No. 0704-0188

1. AGENCY USE ONLY *(Leave blank)*	2. REPORT DATE September 2017	3. REPORT TYPE AND DATES COVERED Master's thesis

4. TITLE AND SUBTITLE SHORT-RANGE ACOUSTIC PROPAGATION USING MOBILE TRANSMITTERS UNDER ARCTIC ICE COVER	5. FUNDING NUMBERS
6. AUTHOR(S) Liam J. Doyle	
7. PERFORMING ORGANIZATION NAME(S) AND ADDRESS(ES) Naval Postgraduate School Monterey, CA 93943-5000	8. PERFORMING ORGANIZATION REPORT NUMBER
9. SPONSORING /MONITORING AGENCY NAME(S) AND ADDRESS(ES) N/A	10. SPONSORING / MONITORING AGENCY REPORT NUMBER

11. SUPPLEMENTARY NOTES The views expressed in this thesis are those of the author and do not reflect the official policy or position of the Department of Defense or the U.S. Government. IRB number ____N/A____.

12a. DISTRIBUTION / AVAILABILITY STATEMENT Approved for public release. Distribution is unlimited.	12b. DISTRIBUTION CODE

13. ABSTRACT (maximum 200 words)

Using mobile acoustic transmitters, acoustic propagation over short ranges was evaluated. Four Expendable Mobile ASW Training Targets (EMATTS) were deployed over two separate days to run at depths of 183, 91, and 46 meters. Emitted frequencies in the bands of 950 to 1150 hertz and 2800 to 3000 hertz were recorded by omnidirectional receivers at ranges out to 10 kilometers. Sound speed profile data was also measured on site. Transmission loss models were created as a baseline at the various depths, ranges and frequencies. The recorded acoustic data was then analyzed to provide measured transmission loss profiles, including variability at range, in order to provide a comparison to the modeled data.

A significant finding was the inability of the modeling software to accurately predict the surface water/ice scattering and absorptive effects on transmitted sound. In addition, sound speed variability by range (usually considered range-independent over short distances) was shown to have a strong effect on transmission. This was demonstrated by very large variances in received sound level (on the level of 30 to 40 decibels) at the same range and depth but different directions.

14. SUBJECT TERMS Arctic, Beaufort Sea, acoustic propagation, transmission loss, sound speed profile, EMATT, bellhop, modeling	15. NUMBER OF PAGES 87
	16. PRICE CODE

17. SECURITY CLASSIFICATION OF REPORT	18. SECURITY CLASSIFICATION OF THIS PAGE	19. SECURITY CLASSIFICATION OF ABSTRACT	20. LIMITATION OF ABSTRACT
Unclassified	Unclassified	Unclassified	UU

NSN 7540-01-280-5500 Standard Form 298 (Rev. 2-89) Prescribed by ANSI Std. 239-18

THIS PAGE INTENTIONALLY LEFT BLANK

Approved for public release. Distribution is unlimited.

SHORT-RANGE ACOUSTIC PROPAGATION USING MOBILE TRANSMITTERS UNDER ARCTIC ICE COVER

Liam J. Doyle
Major, Royal Canadian Air Force
B.Eng., Royal Military College of Canada, 2005

Submitted in partial fulfillment of the
requirements for the degree of

MASTER OF SCIENCE IN PHYSICAL OCEANOGRAPHY

from the

NAVAL POSTGRADUATE SCHOOL
September 2017

Approved by: John Joseph
Thesis Advisor

D. Benjamin Reeder
Co-Advisor

Peter Chu
Chair, Department of Oceanography

THIS PAGE INTENTIONALLY LEFT BLANK

ABSTRACT

Using mobile acoustic transmitters, acoustic propagation over short ranges was evaluated. Four Expendable Mobile ASW Training Targets (EMATTS) were deployed over two separate days to run at depths of 183, 91, and 46 meters. Emitted frequencies in the bands of 950 to 1150 hertz and 2800 to 3000 hertz were recorded by omnidirectional receivers at ranges out to 10 kilometers. Sound speed profile data was also measured on site. Transmission loss models were created as a baseline at the various depths, ranges and frequencies. The recorded acoustic data was then analyzed to provide measured transmission loss profiles, including variability at range, in order to provide a comparison to the modeled data.

A significant finding was the inability of the modeling software to accurately predict the surface water/ice scattering and absorptive effects on transmitted sound. In addition, sound speed variability by range (usually considered range-independent over short distances) was shown to have a strong effect on transmission. This was demonstrated by very large variances in received sound level (on the level of 30 to 40 decibels) at the same range and depth but different directions.

THIS PAGE INTENTIONALLY LEFT BLANK

TABLE OF CONTENTS

LIST OF FIGURES

LIST OF TABLES

THIS PAGE INTENTIONALLY LEFT BLANK

LIST OF ACRONYMS AND ABBREVIATIONS

ASW	Anti-Submarine Warfare
AW	Atlantic Water
CBDW	Canadian Basin Deep Water
CPA	Closest Point of Approach
CTD	Conductivity, temperature, depth
DI	Directivity Index
DT	Detection Threshold
EMATT	Expendable Mobile ASW Training Target
GDEM	Generalized Digital Environmental Model
ICEX16	Ice Exercise, 2016
NL	Noise Level
NOAA	National Oceanic and Atmospheric Administration
NSIDC	National Snow & Ice Data Center
NSTM	Near-Surface Temperature Maximum
PML	Polar Mixed Layer
PSW	Pacific Summer Water
PWW	Pacific Winter Water
RL	Received Level
SAR	Search and Rescue
SL	Source Level
SSP	Sound Speed Profile
TL	Transmission Loss
VLA	Vertical Line Array

THIS PAGE INTENTIONALLY LEFT BLANK

ACKNOWLEDGEMENTS

First, I want to thank my amazing wife, Sandy, for her support throughout this academic adventure. Her determination and positivity kept me on track, while her untiring dedication to our two young children motivated and inspired me. She somehow managed to keep me focused on my work while maximizing our family time, and I will never be able to adequately show my appreciation for it.

My gratitude also goes to Professor John Joseph for his guidance throughout this process. He gave me enough rope to keep me interested but knew just how much to rein me in to keep me out of trouble.

In addition, I would like to thank Professor Ben Reeder for sharing his breadth of knowledge and his efforts to point me in the right direction. Translating academic articles into Canadian is difficult for the best of us, but he did a great job.

THIS PAGE INTENTIONALLY LEFT BLANK

I. INTRODUCTION

A. ARCTIC

The Arctic is one of the last bastions of wilderness in the world. The historically unforgiving climate has made the Arctic one of the most remote and dangerous places on Earth. It is sparsely populated, its ocean is under-researched compared to the other world oceans and it is undergoing momentous climatological change. The long-term effects of this climate change are theoretical or unknown, but the immediate effects are already visible. The smallest Arctic sea ice extent ever documented occurred in September 2012 (NSIDC 2012), and, more recently, the smallest average March sea ice extent in recorded history occurred in March 2017 (NSIDC 2017).

This decrease in sea ice extent has allowed for a potential increase in merchant and passenger traffic through the Arctic. In the summer of 2016, the cruise ship Crystal Serenity completed sailing from Alaska to New York through the Northwest Passage; the first for a large luxury passenger vessel (Dennis 2016). The increased access to potential resources in the area have fueled political arguments while highlighting the difficulty in, among other things, asserting control and policing the area as well as maintaining Search and Rescue (SAR) missions in the far north. Even among allies, there are disagreements: for example, the Canada/U.S. dispute over whether the waters of the Northwest Passage are Canadian internal waters or an international waterway (Sevunts 2017).

As the Arctic becomes more accessible, further commercial and military investment and exploration are inevitable. As outlined in Canada's recent Defence Policy:

> Over time, this interest is expected to generate a corresponding rise in commercial interest, research and tourism in and around Canada's northern territory. This rise in activity will also bring increased safety and security demands related to search and rescue and natural or man-made disasters to which Canada must be ready to respond. (MND 2017)

The higher profile of the Arctic in Canada's (as well as the United States') defense policies means that regional research is a high priority.

The Arctic's water profile seems to be changing, as well. A comparison of a traditional sound speed profile (SSP) in the Arctic (Mellen 1965) and one taken from Ice Exercise 2016 (Nelson 2016) shows a significant difference: the new profile shows the presence of a sound speed channel due to a sound speed peak at a depth of approximately 80 meters. This sound speed channel, as demonstrated in Figure 1, is present between 80–250 meters depth. These differences in sound speed profiles profoundly change how the Arctic is used acoustically and exploited tactically.

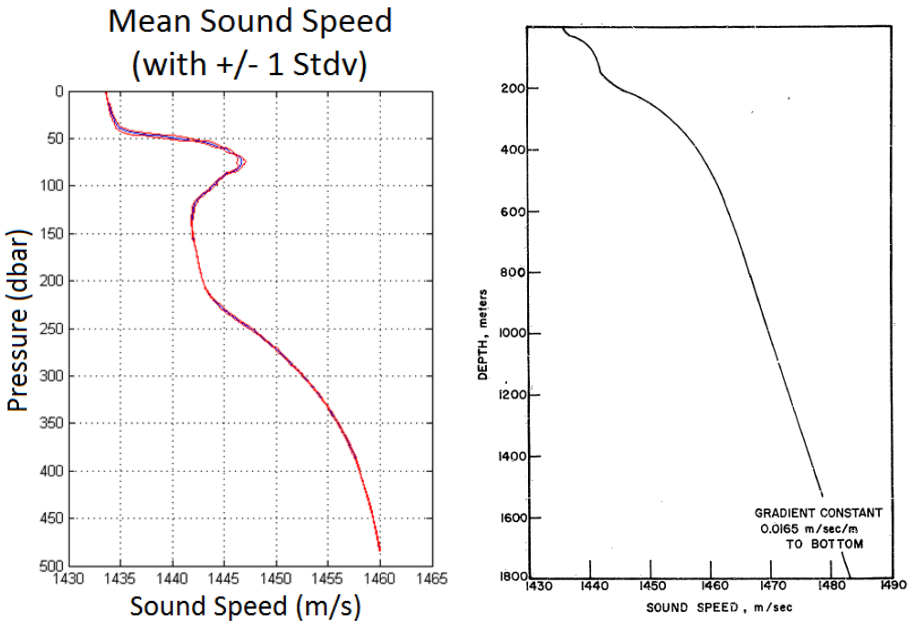

Figure 1. Difference between ICEX SSP (left) and historical Arctic SSP (right). Source: Nelson (2016) and Mellen (1965).

B. SHORT-RANGE ACOUSTICS

Acoustic research has been underway in the Arctic since the 1950s, initiated by the Canadian, Soviet and American militaries. The first research papers and articles were released to the public in the early 1960s (Hutt 2012). The research focused on long-range acoustics: using hydrophones deployed under the sea ice to measure explosive charges at various ranges (Merklinger 2015). This research on long-range acoustics was primarily focused on detection and tracking of nuclear submarines under Arctic sea ice. As

technology improved, however, submarines became quieter and the ranges to detection became shorter. The development of modern submarines has resulted in increased costs with respect to quieting; the cost for each decibel decrease in noise or decibel increase in detection threshold is becoming exponentially higher. This has led to a focus on different detection techniques, including low-frequency active sonar, which had previously been unworkable due to the issues with bearing and range resolution. However, increases in computer processing ability have made these technologies applicable for the tactical level (Clark 2015).

The need to study short-range acoustics in the Arctic is two-fold: firstly, the increased shipping traffic and access to resources due to a drop in Arctic ice cover means the potential for conflict increases. Secondly, the ability to use low- to medium-frequency active sonar over relatively short ranges increases the tactical ability of units to detect and track undersea contacts. Understanding how the changing climate is affecting the sound-speed profile, how ice cover affects acoustic propagation in the near-surface layers and how to accurately measure and predict this acoustic propagation will continue to improve the ability to use the Arctic operationally.

The purpose of this thesis is to study not only range dependent transmission loss, but also azimuthal dependence of transmission loss by using a mobile transmitter. This will better allow us to predict the Arctic Ocean's environmental parameters, and use short-range acoustics to exploit this changing environment for tactical and operational purposes.

THIS PAGE INTENTIONALLY LEFT BLANK

II. BACKGROUND / THEORY

A. THE SONAR EQUATION

The sonar equations provide a good explanation for how sound is produced, travels and is received underwater. They were developed during World War II to determine both the expected maximum range of a sonar as well as a means to develop and test sonar equipment. For the purposes of this experimental data, only the passive sonar equation will be used (an active sonar equation also exists but is inapplicable in this thesis). The passive sonar equation is (Urick 1983):

$$SL - TL = NL - DI + DT \tag{1}$$

The level of sound from the source is represented by the source level, SL, and is referenced at a unit distance from the source; generally, 1 meter. As the sound spreads out from the source to the receiver, the sound level is diminished by transmission loss, TL. Therefore, the received sound (received level, RL) will be represented by the source level minus the transmission loss, SL – TL. Conversely, if we have a measured RL and a documented SL, we can calculate the TL from the following equation:

$$TL = SL - RL \tag{2}$$

The background noise in the water is the noise level, NL. This is reduced if we have a directional receiver; that is, a receiver pointing in the direction of the sound source. This property is known as the directivity index, DI. The detection threshold, DT, is the signal-to-noise ratio that just allows detection of the target. The detection threshold is based on the probability of false alarm and probability of detection, which are determined by the equipment and the operator (Urick 1983).

B. DOPPLER SHIFT

As a target that is emitting a tonal moves relative to a receiver, the received frequency will be shifted either up or down, depending on whether the target is approaching or moving away from the receiver, as shown in Figure 2. If the target is approaching the receiver, the received frequency will be higher than the actual source

frequency. As the target passes (its path is tangential to the receiver) the received frequency will be exactly the same as the source frequency; this is the CPA. After passing, the received frequency will be lower than the source frequency (Kapolka 2016). This is mathematically demonstrated by the Doppler shift equation (Medwin 2005):

$$f_r = f_0 * \frac{(c + u * \cos\theta_s)}{(c + v * \cos\theta_r)} \tag{3}$$

For Equation 3: f_r is the received (shifted) frequency, f_0 is the source (transmitted) frequency, c is the speed of sound, u is the speed of the source, v is the speed of the receiver (positive if towards the source, negative if away from the source). For the angles: θ_s is the angle between the source track and a direct line between the source and the receiver, and θ_r is the angle between the receiver track and a direct line between the receiver and the source. For this application, both the source and the receiver are at or near the same depth (Medwin 2005).

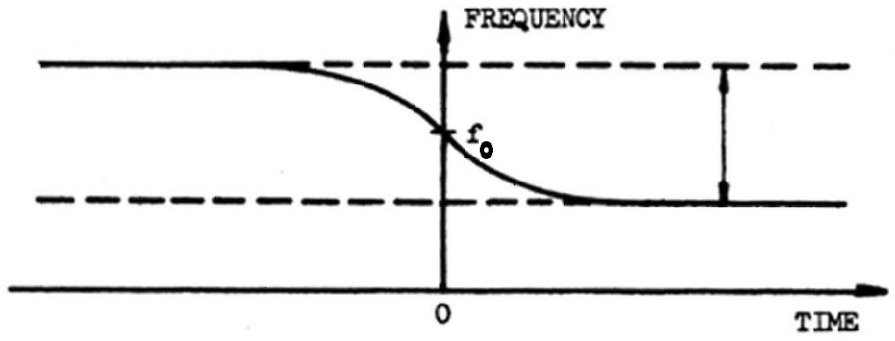

The source frequency is shown as f_0. The frequency to the left of f_0 is higher, showing the target is approaching the receiver. When the frequency reaches f_0, the target is at CPA to the receiver. After CPA, the frequency is lower than f_0, showing the target is moving away from the receiver.

Figure 2. Frequency shift of a target passing a stationary receiver. Source: Kapolka (2016).

C. OCEANOGRAPHY IN THE ARCTIC

The research was conducted in the Beaufort Sea, a part of the Canadian Basin. The Arctic Ocean itself has many interesting properties that contribute to its unique acoustic characteristics.

1. Overview / Water Masses

The Arctic Ocean is a mediterranean sea that is bordered by land on all sides, with inflow from the Pacific (through the Bering Strait) and the Atlantic (through the Fram Strait and Barents Sea) and outflow to the Atlantic (through the Canadian Archipelago, Nares Strait and Fram Strait). In the Canadian Basin, there is a unique vertical structure. The freezing of seawater results in brine rejection, where cold, salty water sinks from the surface and creates deep water. In the summer, the melting ice causes a rise in the fresh water content, though the river runoff is a more significant contributor to the low salinity in the Arctic Ocean. Relatively cold, salty water from both the Pacific and the Atlantic is present throughout the Arctic Ocean. Since the Pacific is less dense than the Atlantic (less saline) the Pacific water rests on top of the Atlantic water (Talley et al. 2011).

In the Canadian Basin, the surface layer is called the Polar Surface Water, extends down to around 200 meters, and is made up of the Polar Mixed Layer (PML), Pacific Summer Water (PSW) and Pacific Winter Water (PWW). In the summer, the presence of a near surface temperature maximum (NSTM), shown in Figure 3, adds to the complexity of the vertical water profile in the Canadian Basin (Jackson et al. 2010). The PML is relatively fresh (28-34 psu) from river runoff and melted sea ice (in the summer), and extends from the surface to 25–50 meters. PSW extends from the PML to a depth of 70–130 meters, where another temperature maximum is encountered. The strong gradient between the PML and the PSW can cause highly variable sound speeds due to mixing and turbulence (Nelson 2016). Below the PSW is the PWW, down to a depth of approximately 200 meters. Below the PWW is the Atlantic Water (AW), which again has a temperature maximum, and extends to a depth of around 1000 meters. Below the AW is the deep water, from 1000 meters to the bottom (Talley et al. 2011).

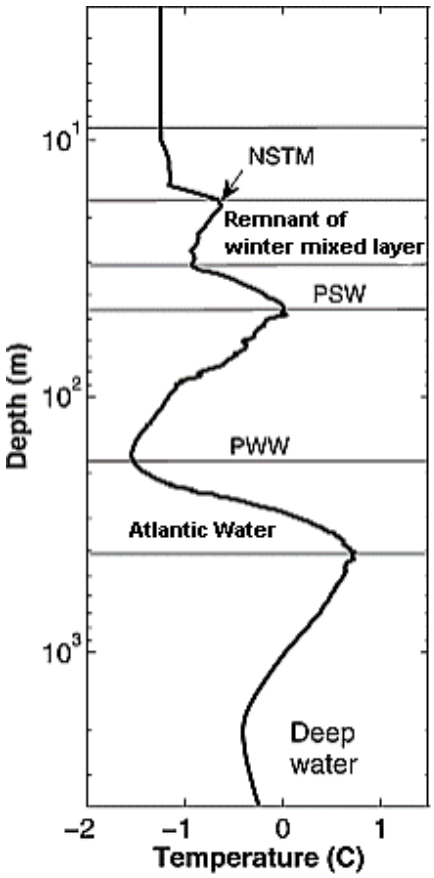

Figure 3. Temperature profile of the Canadian Basin indicating different layers. Source: Jackson et al. (2010).

2. Sea Ice

The Arctic Ocean is unique because it is a large ocean basin that has permanent ice cover. The properties of sea ice mean that it is the most important defining feature in terms of acoustics in the undersea environment. This is especially true due to its movement, as well as the fact the ice cover changes so dramatically with the seasons. Ice cover strongly affects the ambient noise level (NL in Equation 1) both positively and negatively. The presence of ice cover means that normal environmental noise such as wind and wave noise is muted or eliminated, but the ice itself adds noise as ice masses interact with each other, as the ice cracks and even as ice masses push together and cause ridging (Hutt 2012). The ice also greatly limits shipping, resulting in much lower ambient noise from shipping sources. Due to

these factors, the under ice ambient noise in the Arctic can be up to 30 dB higher, or even 20 dB lower, than noise in the same area without ice, as demonstrated in Figure 4.

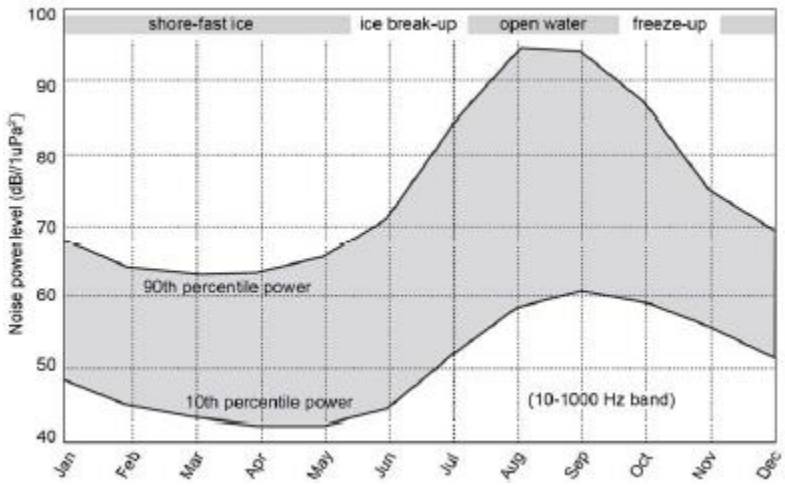

Figure 4. Ambient noise variability due to ice cover in the Arctic. Source: Hutt (2012).

Ice also greatly increases the scattering of acoustic energy. The ice provides for a large and highly variable level of scatter due to the interface of ice and water at the surface. The highly variable nature of the scattering from the ice means that it is extremely difficult to create a reliable model for predicting reverberation. Ice can also lessen volume scattering in the ocean: the ice blocks a large amount of the sunlight, resulting in much less biomass under the ice, which results in less volume-scatter that normally occurs in the water column. This lower level of volume scattering may be in the magnitude of 15-20 dB less than in other world oceans (Hutt 2012).

3. Spiciness

Water density at a given depth is effectively defined by temperature and salinity. Cold, fresh water can be the same density as warm, salty water, and therefore, they can be at the same or similar depths. Sound speed increases with temperature and salinity, so sound propagates quicker through warm, salty water than it does through cold, fresh water. This acoustic property (different sound speeds in the same isopycnal) is known as

spice, where cold and fresh water is called “weak spice” and warm and salty water is called “strong spice” (Colosi 2016). These areas of weak and strong spice cause sound speed anomalies throughout the water column. The PML, which can contain fresh runoff or ice melt as well as brine-rejected highly saline water, is a prime location for areas of strong and weak spice and therefore sound speed anomalies.

III. EXPERIMENTAL SET-UP

A. ICEX16

All research was conducted during Ice Exercise 2016 (ICEX16) in the Beaufort Sea, from 10 March 2016 to 12 March 2016. A detailed description of ICEX16 is recorded in Lieutenant Mitchell Nelson's 2016 thesis (Nelson 2016).

B. EQUIPMENT

The receivers used in this experiment were Acousonde acoustic recorders. Acousondes are manufactured by Acoustimetrics, a subsidiary of Greeneridge Sciences, Inc. They are described as "a miniature, self-contained, autonomous acoustic/ultrasonic recorder designed for underwater applications" (Acoustimetrics 2013). Fitted with lithium batteries, the recorders are designed to be reusable, programmable, and fully sealed for various uses, from tagging marine life to using as general acoustic recorders in the field. They have been tested down to -17°C and maintained battery life for 13 hours at that temperature. For this experiment, they were protected from the much colder air temperatures until deployed into the water.

The mobile transmitters used were MK39 Expendable Mobile Anti-Submarine Warfare (ASW) Training Targets (EMATTs) developed by Lockheed. They are course- and speed-programmable, and can emit tonals over a broad range of low- to mid-frequencies (Lockheed Martin 2013). Navigation is by magnetic compass and uses dead reckoning. This means it is susceptible to ocean currents causing it to drift. The EMATT is engaged by saltwater and circles to configure its compass, then dives to the mission depth once it is on course. Programmed speed is determined using propeller RPM, so speed in dive and ascent is variable.

The conductivity, temperature, and depth (CTD) were measured using a Sea-Bird Scientific SBE 19 SeaCAT Profiler CTD. It is rated for a depth of 1000 m, and is usually equipped with a pump for continuous water measurement. In this experiment, the pump was omitted, and water flow was obtained through raising and lowering the CTD through the water column.

C. CONDUCT

The Acousondes were set up in three locations: two vertical line arrays (VLAs) with two receivers on each were deployed in the field and a single receiver at the EMATT deployment location. All Acousondes were programmed to sample at a rate of 25.8 kHz. Both VLAs had an Acousonde at 183m (initial EMATT programmed depth) and 45m (just above the variable sound layer). The Acousonde at the deployment location was set at a depth of 125m. The Acousonde numbers and associated VLAs and depths can be found in Table 1.

Table 1. Acousonde deployment data

Acousonde Number	VLA	Depth (m)
A020	1	183
A023	2	183
A044	EMATT drop location	125
A042	1	45
A045	2	45

VLA 1 was set up to the east, at 83.5 degrees true and 2820 meters relative to the deployment location. VLA 2 was set up to the west at 251.2 degrees true and 1141 meters relative to the deployment location. The deployment position, bathymetry as well as the two VLA positions are in Figure 5. The VLAs were set up in basically a straight line with the deployment location array. The sound speed profile was measured three times during EMATT deployment in total, for both days.

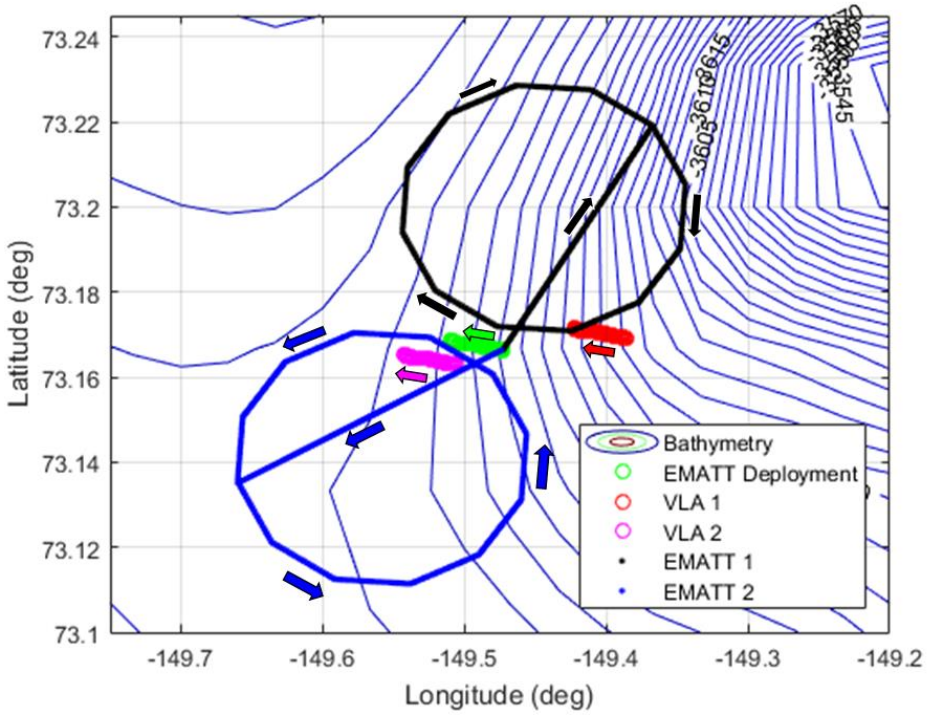

Both VLA 1 and 2, the EMATT deployment location as well as the projected EMATT tracks (including variation), are shown. VLA 1, 2 and the deployment location show the ice movement over the entire 10-hour EMATT run time.

Figure 5. Experimental Set-up for 12 March

For both 10 March and 12 March, two EMATTs were deployed. They were programmed to drive directly away from the deployment location in relatively opposite directions, at 3 knots, and then complete 3 circles of 3 hours each, at various depths, for a total run time of 10 hours. These "circles" were actually 12 legs of 15 minutes each, with a 30 degree turn at the end of each leg, creating a dodecagon. EMATT 1 was programmed to do clockwise circles, while EMATT 2 was programmed to do counter-clockwise circles. For example, EMATT 1 was programmed to start at a magnetic heading of 030, and at the end of 1 hour turn clockwise 105 degrees to a course of 135 degrees for 15 minutes, then turn to 165 degrees for 15 minutes, etc. Programmed course, depth and frequency emitted can be seen in Tables 2 and 3, and the predicted EMATT courses are shown in Figure 5. Average magnetic variation at the deployment location was 19.3 degrees east on 10 March, and 18.9 degrees east on 12 March (NOAA 2017).

For the first and second circle, each EMATT emitted two distinct tonals; the rest of the run, only a single frequency tonal was emitted. As well, every 57 seconds, for 3 seconds, a broadband LFM sweep was emitted (effectively, for 3 seconds per minute). For EMATT 1, this was from 700Hz to 1400 Hz, and for EMATT 2, this was 2300 Hz to 3000 Hz.

Table 2. Programmed courses, depths and frequencies for EMATT 1

Time After Drop (HH:MM)	**Course (Degrees Magnetic)**	**Depth (feet)**	**Frequency (Hz)**
00:00	030	600	950
01:00	135	600	950 and 1050
01:15	165	600	950 and 1050
…	…	600	950 and 1050
04:00	135	300	950 and 1150
04:15	165	300	950 and 1150
…	…	300	950 and 1150
07:00	135	150	950
07:15	165	150	950
…	…	150	950
09:45	105	150	950

Table 3. Programmed courses, depths and frequencies for EMATT 2

Time After Drop (HH:MM)	Course (Degrees Magnetic)	Depth (feet)	Frequency (Hz)
00:00	240	600	2800
01:00	135	600	2800 and 2900
01:15	105	600	2800 and 2900
…	…	600	2800 and 2900
04:00	135	300	2800 and 3000
04:15	105	300	2800 and 3000
…	…	300	2800 and 3000
07:00	135	150	2800
07:15	105	150	2800
…	…	150	2800
09:45	165	150	2800

D. PROCESSING SOFTWARE / ANALYTIC METHOD

All acoustic data was processed using MATLAB software. Acoustic models were developed using the modeling tool Bellhop in MATLAB. The sound speed profiles were created using measured data prior to, during or after the EMATT runs. Because CTD data was only available down to near 500m depth, the U.S. Navy's Generalized Digital Environmental Model (GDEM) data was used below 500m. With the sound speed profile, propagation paths were modeled in order to profile the expected TL. Using Equation 2, the actual measured TL was then compared to the modeled TL.

THIS PAGE INTENTIONALLY LEFT BLANK

IV. DATA ANALYSIS

A. INITIAL ASSUMPTIONS

Some initial assumptions were made in order to proceed with the analysis of the experimental data. First, while CPA calculations would enable a rather precise location of the EMATTs on their straight leg past the Acousondes, once they start turning in circles the positional data from acoustic measurements alone would prove almost impossible within the scope of this paper. The assumption is, then, that there is minimal drift, and that the EMATTs behaved as programmed.

The second initial assumption is that the EMATTs remained relatively near the deployment point, orbiting around their drop area to calibrate their compasses, then diving to depth once they are on the programmed track. Doppler data provides the radius of the initial calibration circle, at which point the uncertainty of their position will be taken into account. Diameters of approximately 30–40 meters are expected based on experience.

B. LOCATION

The GPS data was recorded using different recorders. The actual Ice Camp SARGO positional data was recorded on the hour, while the location data recorded at the EMATT deployment point and both VLAs was recorded much more sporadically, and at different intervals. In order to compile the location data and make it useful in determining EMATT range data, the GPS data from the ice camp was interpolated on the second, and the VLA 1, 2 and EMATT deployment data was used (when present) to determine relative range and distance from the ice camp as well as the speed of the ice while the EMATT was running. While position data can be variable due to ridging and shifting ice, the error was almost negligible. The relative positions of the EMATT deployment, VLA 1 and VLA 2 can be found in Table 4. The ice on 10 Mar travelled at an average velocity of 0.36 kts at 271 degrees true. On 12 Mar, the ice travelled at an average velocity of 0.07 kts at 282 degrees true.

Table 4. Positions relative to Ice Camp SARGO

Location	Range (m)	Bearing (Degrees True)
EMATT Deployment	228 +/- 4.2	234.2 +/- 1.9
VLA 1	2623 +/- 5.6	85.9 +/- 0.7
VLA 2	1362+/- 5.5	248.4+/- 0.3

C. ACOUSONDE DATA AND EMATT TRACK

The spectrogram of the acoustic data was produced. MATLAB was used to filter and display the data. Figures 6 and 7 show data from EMATT 1 on 10 March. These spectrogram figures show the frequency received versus time; the color of the figure is representative of the received level (RL) in decibels re 1μPa. The frequency emitted by EMATT 1 was a 950 Hz tonal. The EMATT did not behave in an expected manner, as shown in Figures 6 and 7, both because of the almost 30-minute compass calibration, as well as the relatively far CPA as evidenced by the shallow frequency gradient across 950 Hz in Figure 7.

Figures 8 and 9 show data from the same Acousonde (A020), viewing the same frequency band, on 12 March. The Doppler shift is present as well, and it is clear that in Figure 8, the EMATT calibrated quickly; only 3 minutes 31 seconds. The dive occurring at a higher speed than the rest of the mission is also apparent. This can be seen from the higher frequency (952 Hz) at around 06:50 in Figure 9. The angle of the received sound through the central frequency also suggests a closer CPA, much more in line with the predicted EMATT track than the data from 10 March. The spectrograms for all Acousondes, at both 950 Hz and 2800 Hz, can be found in Appendix A.

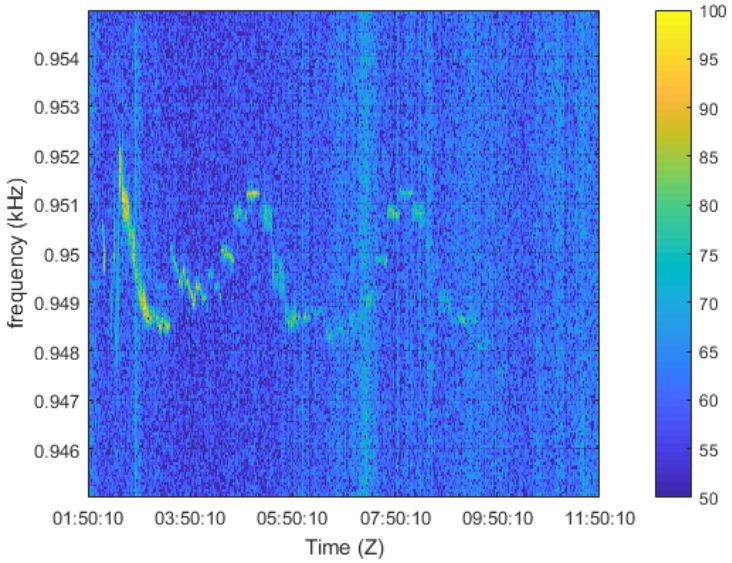

The received frequencies below and above the central frequency of 950 Hz show us the behavior of the EMATT relative to the Acousonde. The Doppler shift is clearly seen as the EMATT travels past the Acousonde early in the run (02:20-03:20), and then circles the Acousonde throughout the next 9 hours.

Figure 6. 10 March spectrogram data from Acousonde A020 for EMATT 1 at 950 Hz

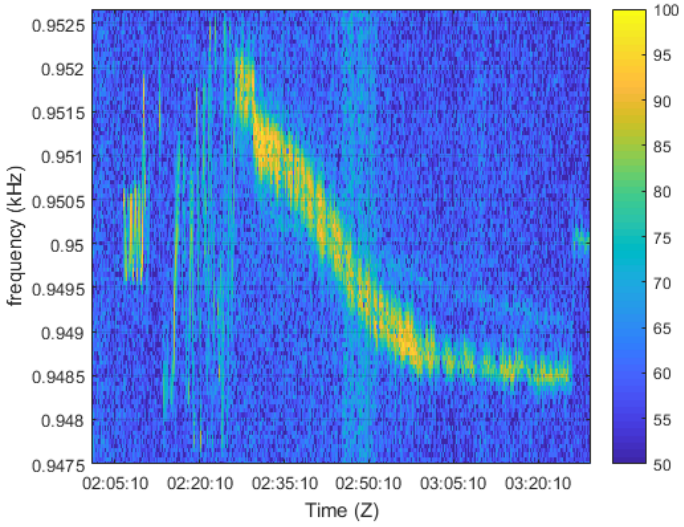

An almost 30-minute compass calibration period can be seen on the left side of the figure. Also, the relatively shallow angle of the frequency change over the central frequency of 950 Hz was not expected based on predicted EMATT tracking relative to the Acousonde.

Figure 7. 10 March zoomed in Figure 6 for EMATT 1 deployment

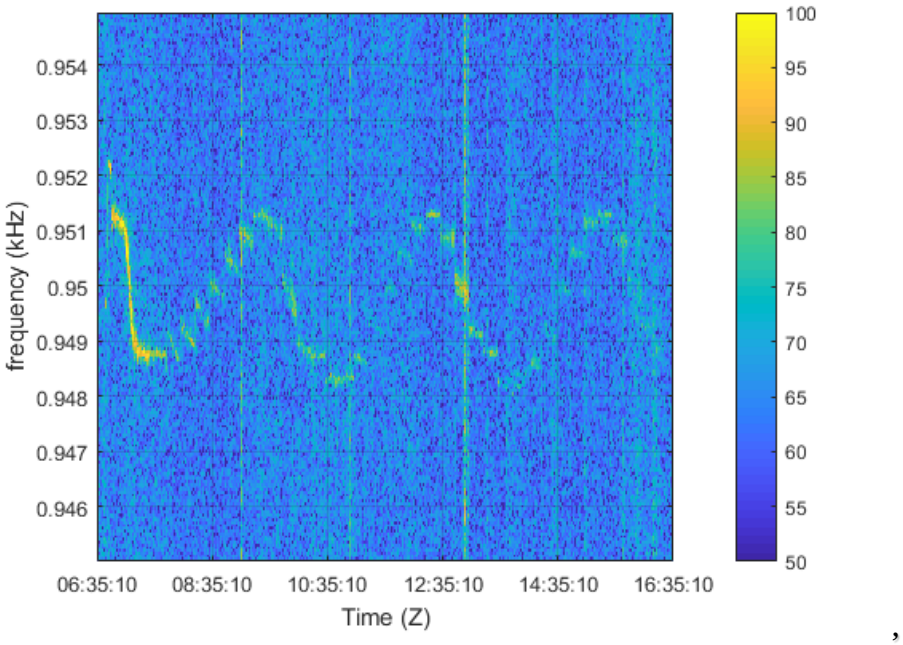

Figure 8. 12 March spectrogram data from Acousonde A020 for EMATT 1

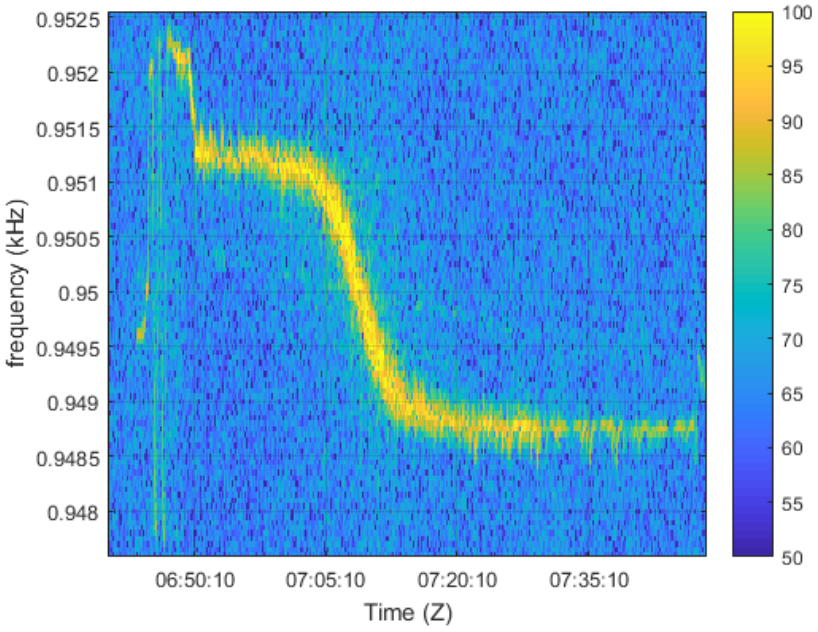

The short calibration time, the increased speed of the dive and a sharper CPA angle provide much more usable information.

Figure 9. 12 March magnified spectrogram data from Acousonde A20 during EMATT 1 deployment

Extracting the Doppler data information from the Acousonde received data was accomplished using Equation 3, as well as the formula and MATLAB program developed by Lieutenant Commander Chris Bade in his insightful thesis (Bade 2017). Using the Doppler data, speed of each EMATT on each day was calculated, as well as CPA from the closest Acousonde. This data is compiled in Table 5.

Table 5. Calculated EMATT speeds and CPA

EMATT	SPEED (kts)	CPA (m) [Acousonde]
10 March		
1	4.43	1511 [A020]
2	3.41	290 [A023]
12 March		
1	3.69	454 [A020]
2	3.71	404.5 [A023]

There is a significant difference in calculated speed between EMATT 1 and EMATT 2 on 10 March, as shown in Table 5. While the moving ice definitely plays a part, since it is travelling at a speed of 0.36 kts, the cumulative difference (0.72 kts relative difference between opposite direction EMATTs from the same Acousonde) is not of a great enough magnitude to explain the speed difference of 1.02 kts. The likely solution is that there is a non-negligible drift component; i.e. current.

The presence of drift, which was not measured during the experiment, as well as the long calibration time for EMATT 1, caused unacceptable positional error for the data collected on 10 March. For these reasons, all further analysis will focus on the data collected on 12 March.

Using the CPA and EMATT speed data, as well as the location data for EMATT deployment, initial heading was calculated. Using the programmed data as a template,

and the Acousonde data to determine which side of the Acousonde the CPA was on, the EMATT track was calculated and plotted with time. Figure 10 shows the updated EMATT tracks as calculated. Comparison with Figure 5 shows a rather strong difference from our predicted track, but fits with the acoustic data with respect to Doppler shift, both in direction and angle.

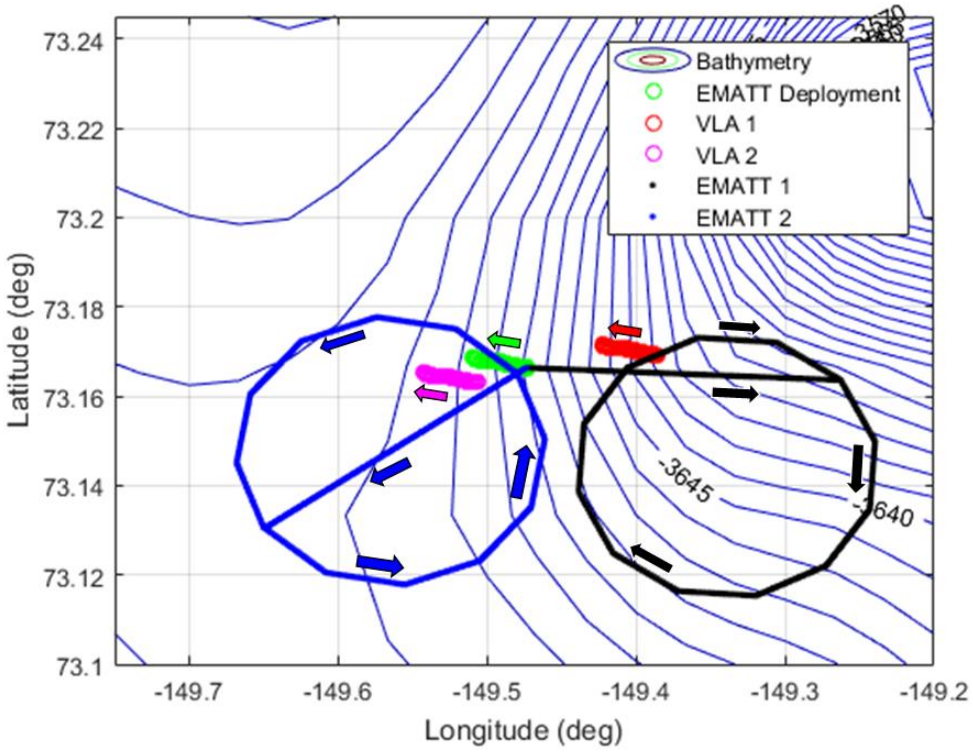

Figure 10. Calculated EMATT tracks for EMATT 1 and 2 on 12 March

D. TRANSMISSION LOSS

1. Sound Speed Profile

On 12 March, EMATT 1 was deployed at 06:43Z and stopped transmitting at 16:30Z. EMATT 2 was deployed at 06:51Z and stopped transmitting at 16:35Z. A CTD cast was taken at 05:30Z, before deployment, and another at 17:24Z, after the EMATT had ceased transmitting. The sound speed profile (SSP) was determined for each cast, and an average was calculated. Both sound speed profiles are shown in Figure 11. The SSPs

are plotted as sound speed versus depth. The GDEM data was plotted to extrapolate the SSP below the CTD data. Figure 12 shows the averaged measured SSP with both CTD and GDEM data down to the bottom at approximately 3650m.

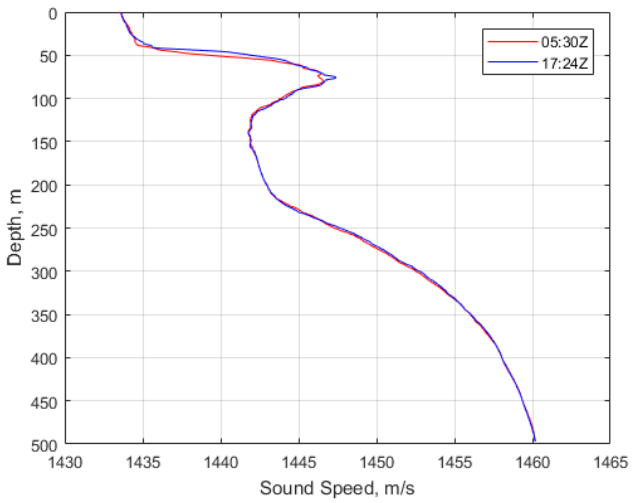

This figure reflects the strong variability around 50-meters depth, and this even extends down to the peak at 80 meters. This variability is temporal and spatial, since the ice (and accompanying CTD measurements) moved throughout the experiment.

Figure 11. Measured SSP data for 12 March

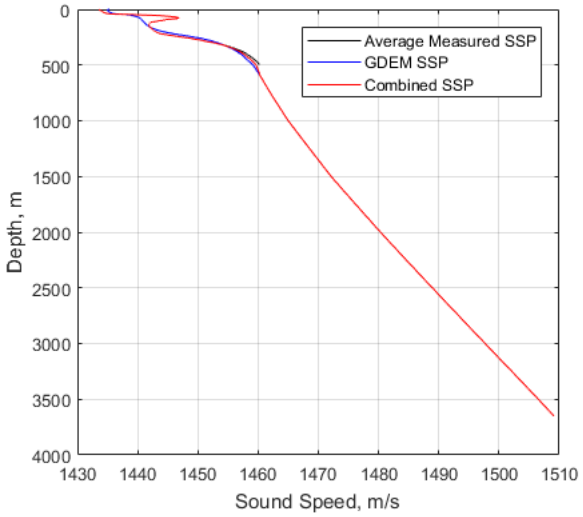

Figure 12. Averaged SSP data with GDEM addition

2. Modeled TL

Using the SSP from Figure 12, the TL was modeled at 950 Hz and 2800 Hz for sources (EMATT) at depths of 183m, 91m and 46m. The same parameters were modeled using each individual CTD cast to determine how the modeled TL changes with the variability. The presence of a shallow sound speed maximum at approximately 80m (as seen in Figure 11) results in a very complicated propagation model. This can be seen in Figures 13, 14 and 15, which are the 2800 Hz tonal at various EMATT depths. The strong upward refracting SSP causes much of the sound to be trapped in the channel, though there is significant surface interaction for all source depths at further ranges. Modeled TL data for the 950 Hz EMATT can be found in Appendix B.

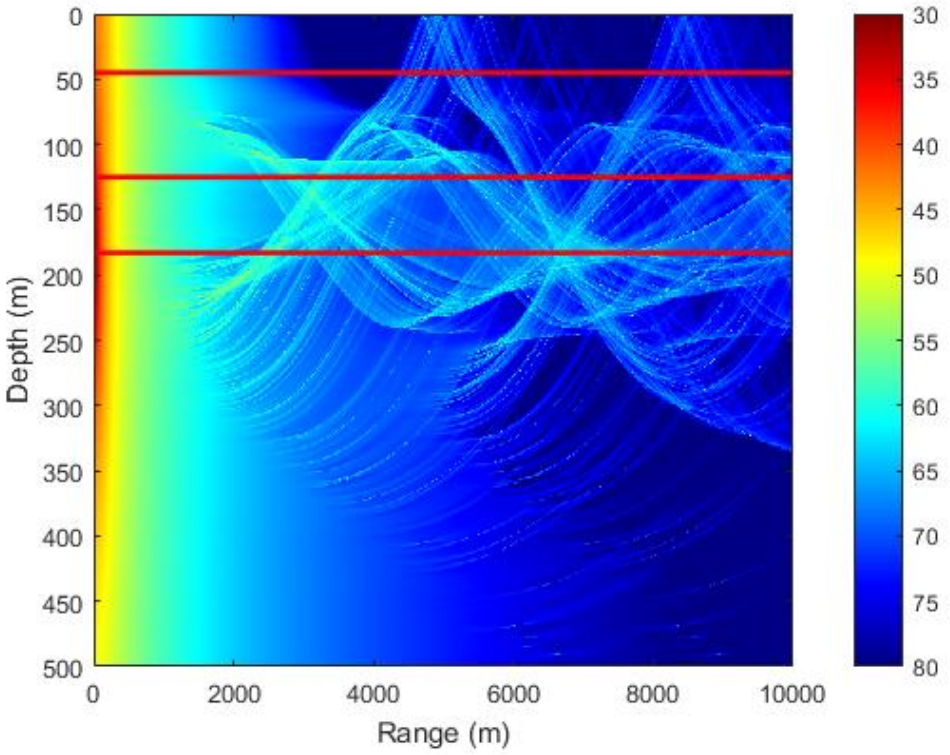

The red lines show the depths at which the Acousonde receivers are. Because the source was mobile, the receivers are represented as lines across range versus point receivers. Strong areas of reception as well as shadow zones can be seen.

Figure 13. Modeled 2800 Hz TL with EMATT at 183m

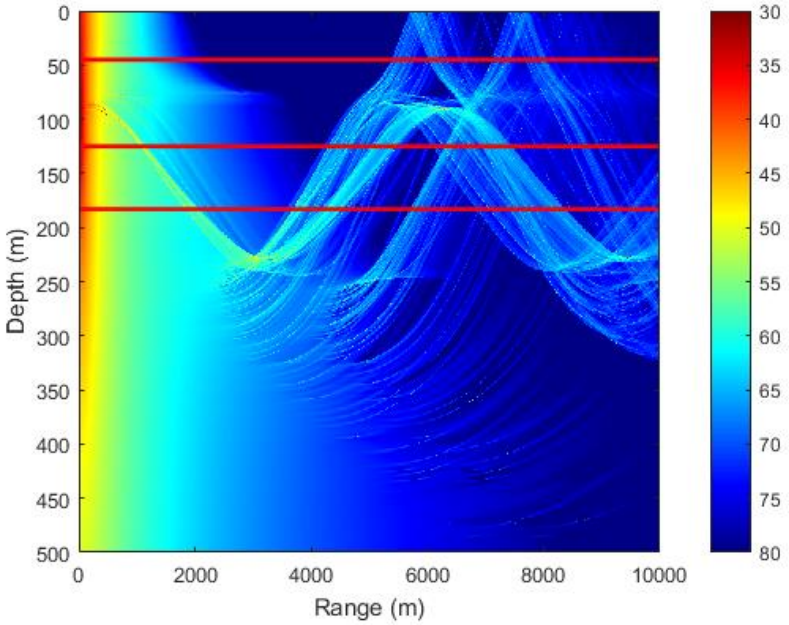

Figure 14. Modeled 2800 Hz TL with EMATT at 91m

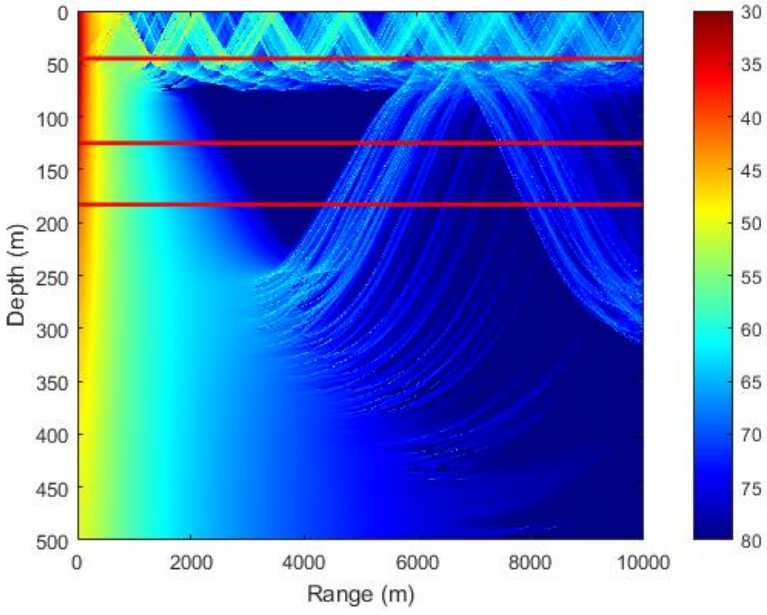

The trapping of sound energy in the surface layer, with the resultant surface interaction, is well demonstrated. Relatively little sound energy is emitted below the layer compared to the other EMATT depths.

Figure 15. Modeled 2800 Hz TL with EMATT at 46m

These modeled TL figures use the averaged SSP. In order to understand the effects of the variability in the SSP, the models were also run with the SSP from the CTDs at 05:30Z and 17:25Z, individually. A good visualization of the difference in TL due to variability can be found in Figure 16. The TL peaks are strongly variable, even when a small change in SSP is modeled. This shows the acoustic sensitivity to small changes in the water column at this gradient. This figure represents the expected TL for the 45m Acousondes (A042 and A045) when the EMATT is at 46m depth. Due to the temporal and spatial variability of the SSP, a highly variable TL plot is expected.

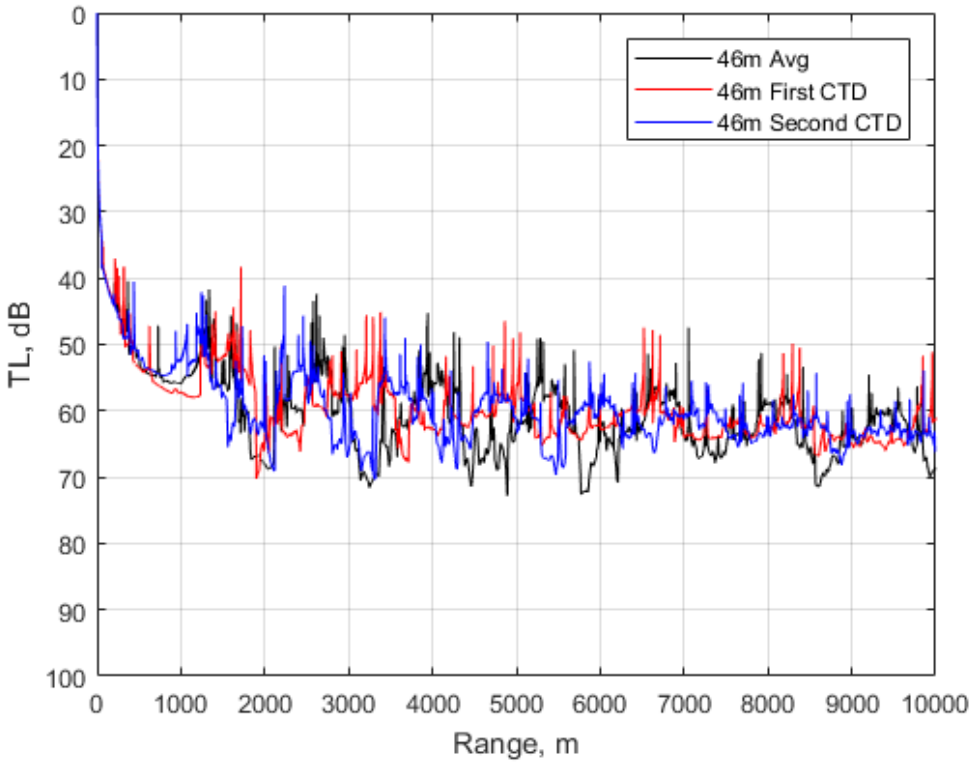

TL using 3 separate sound speed profiles. The red line is the modeled TL for the first CTD at 05:30Z, the blue line is the second CTD at 17:25Z, and the black line is the averaged SSP of both CTDs. This averaged SSP was used to determine the modeled TL in Figures 13–15.

Figure 16. Modeled TL in dB versus range for a 45m Acousonde with EMATT at 46m depth

3. Calculated TL

Using Equation 2, the TL was calculated by subtracting the received level from the source level. The expected source level from an EMATT based on frequency emitted is shown in Figure 17. For the times when 2 tonals were emitted, such as the first and second circles, the SL is halved (3 dB less). Therefore, for 950 Hz, the SL for a single tonal is 148.5 dB (145.5 dB for two tonals) and for 2800 Hz, the SL is 148 dB (145 dB for two tonals).

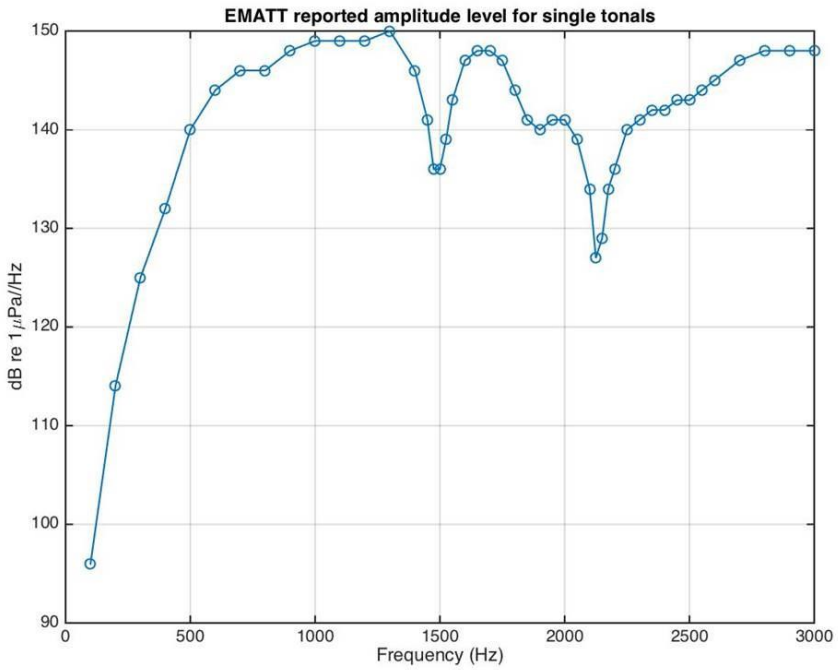

Figure 17. Expected SL at selected frequencies for EMATT

The received level was initially averaged over a 5 second interval, but due to the highly variable SSP and potential scattering effects of the surface ice, the decision was made to average it over a 1 second interval. Analysis of the data showed that when EMATT 1 was supposed to be emitting a 3-second LFM sweep, the EMATT ceased transmitting. For any interval larger than 1 s, this lowered the averaged RL more than

was acceptable. Using a 1-second average and removing values at or below the noise level resulted in a much more accurate, clear plot.

The TL was measured as a function of time, so the predicted EMATT position versus time was calculated. The position of the EMATT relative to each VLA and the "drop point" Acousonde located at the camp as a function of time can be seen in Figures 18–20. This is horizontal range to the VLA, not slant range. For the individual Acousondes where TL versus range was plotted, slant range was used based on the programmed EMATT depth.

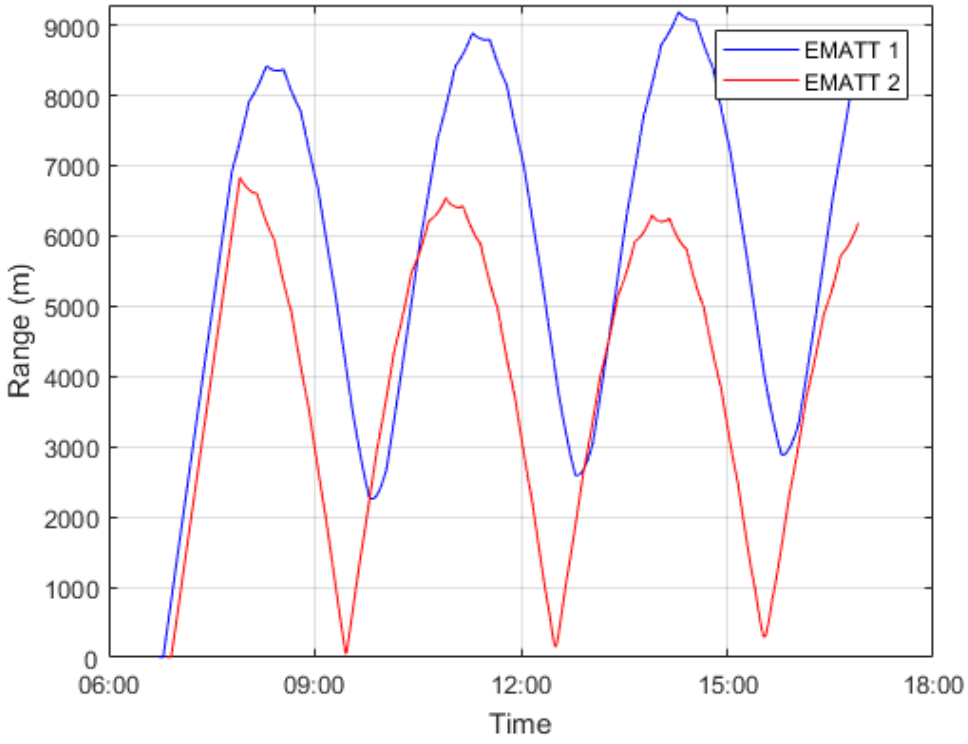

Figure 18. Distance from drop point Acousonde for both EMATTs

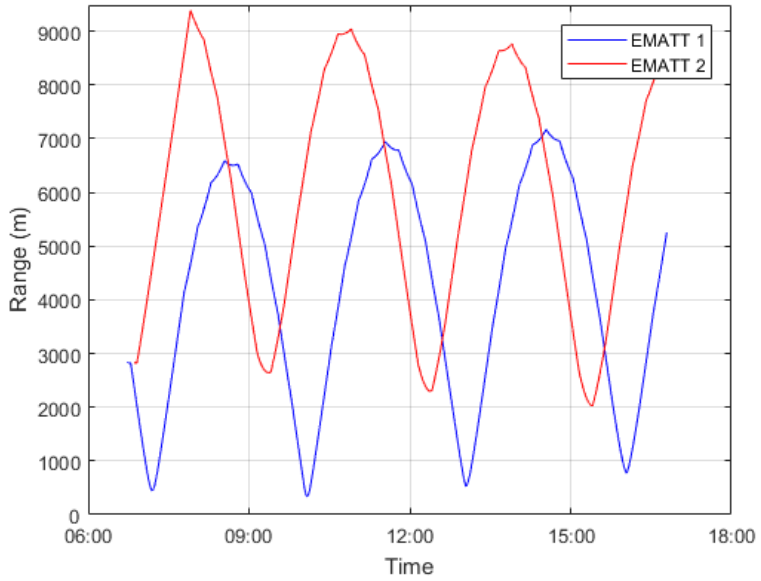

Figure 19. Distance from VLA 1 for both EMATTs

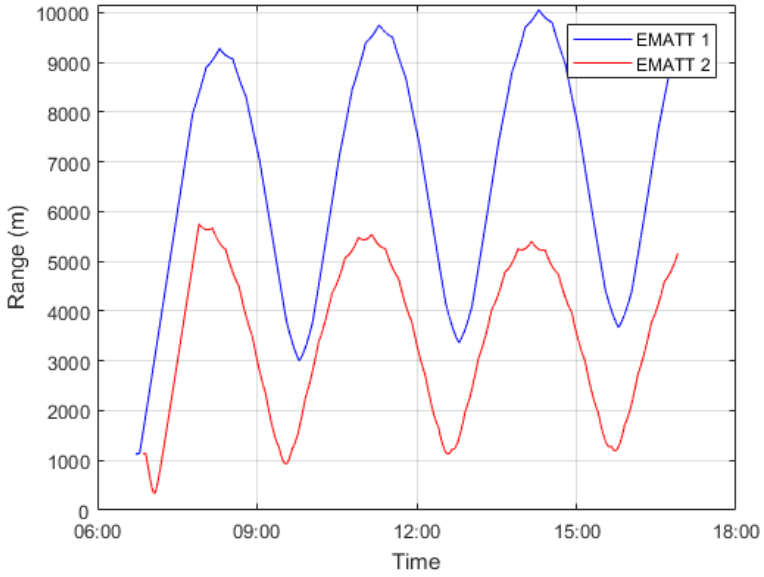

Figure 20. Distance from VLA 2 for both EMATTs

The observed TL versus range for some representative Acousondes and EMATT depths is shown in Figures 21–26. These figures show the measured and modeled TL, plotted in dB, versus the range of the EMATT. The measured data is plotted with the

modeled TL data for the same Acousonde and EMATT depth. General trends show less TL at short ranges, as we would expect. The measured TL as well as the differences between measured and modeled data will be discussed in Chapter V. Figures for measured versus modeled TL for each Acousonde and EMATT depth can be found in Appendix C.

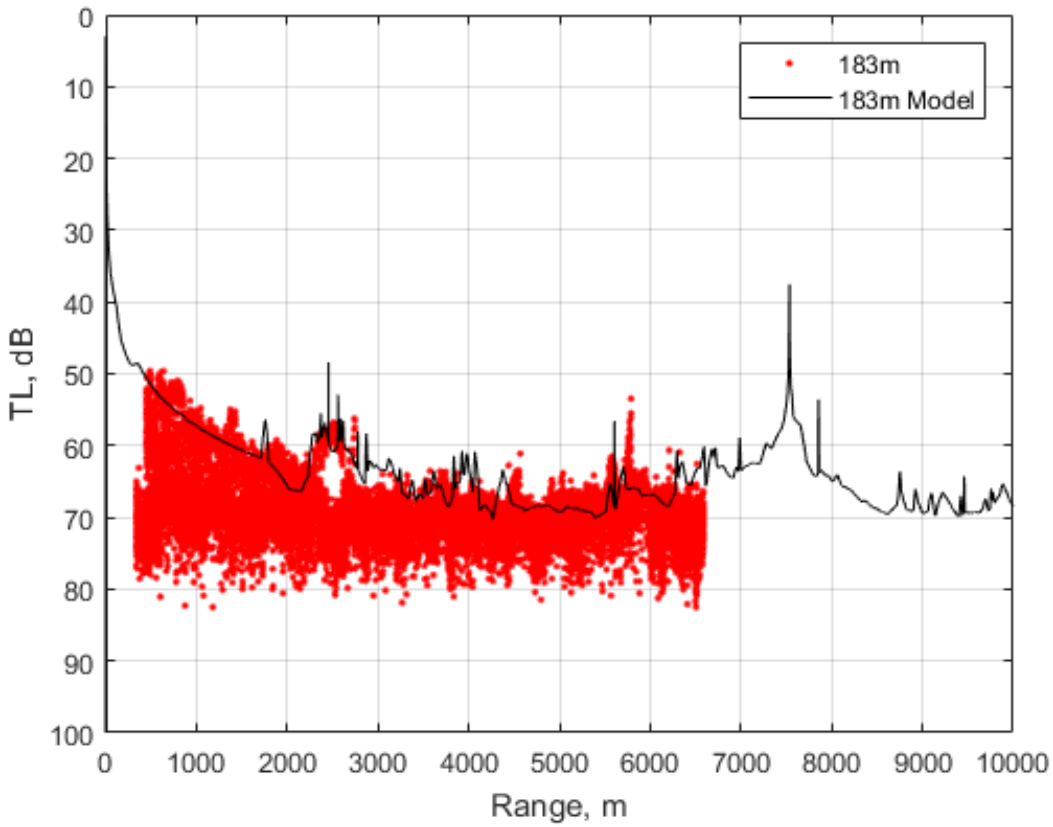

The TL is generally smaller at short ranges, but there are noticeable peaks throughout, specifically at around 2500 meters and 5600 meters for this EMATT/Acousonde combination. Variability is shown to be as high as 30 dB for this frequency. The comparison to the modeled TL shows little in common, other than at short range and both peaks.

Figure 21. A020 (183m) measured and modeled TL, EMATT at 183m, 950 Hz

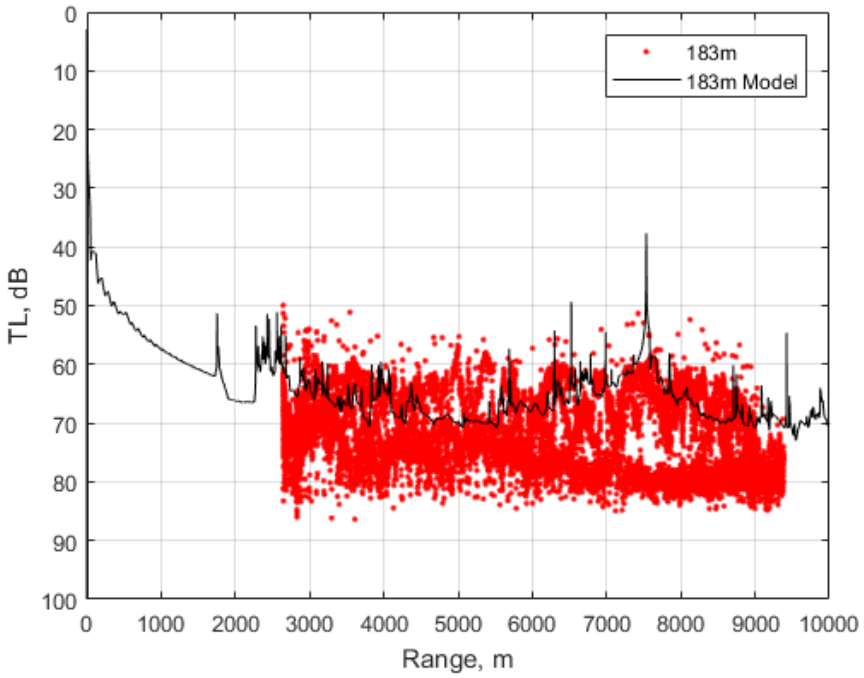

Figure 22. A020 (183m) measured and modeled TL, EMATT at 183m, 2800 Hz

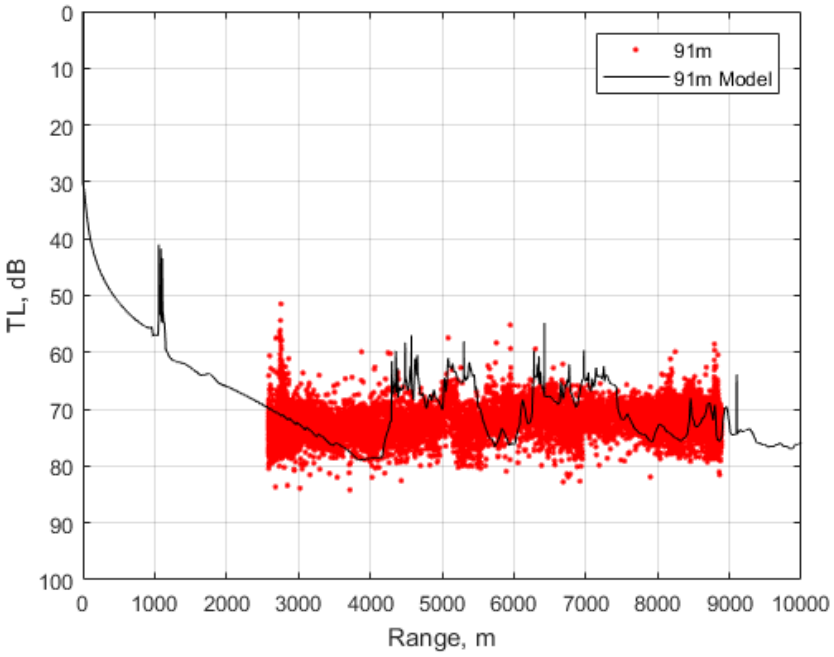

Figure 23. A044 (125m) measured and modeled TL, EMATT at 91m, 950 Hz

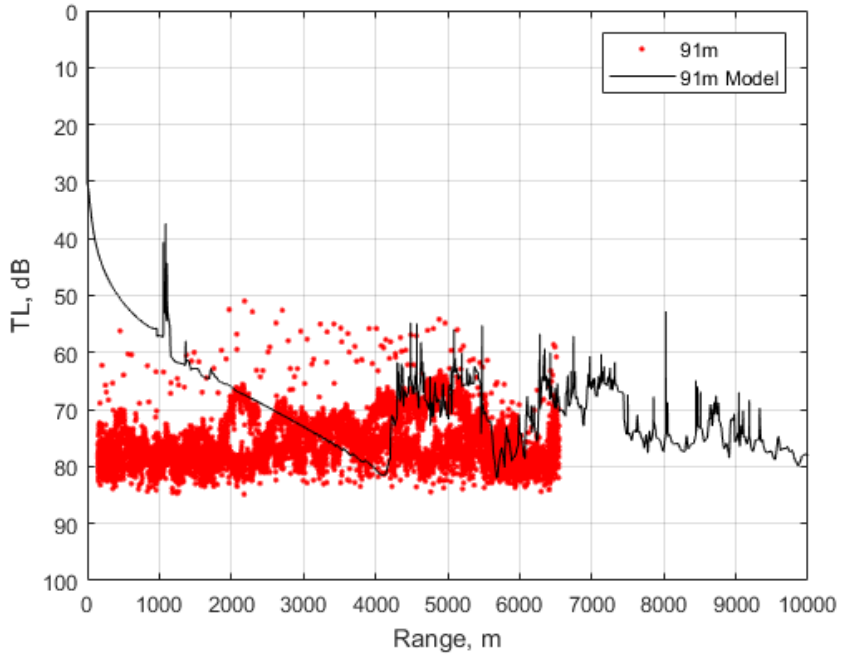

Figure 24. A044 (125m) measured and modeled TL, EMATT at 91m, 2800 Hz

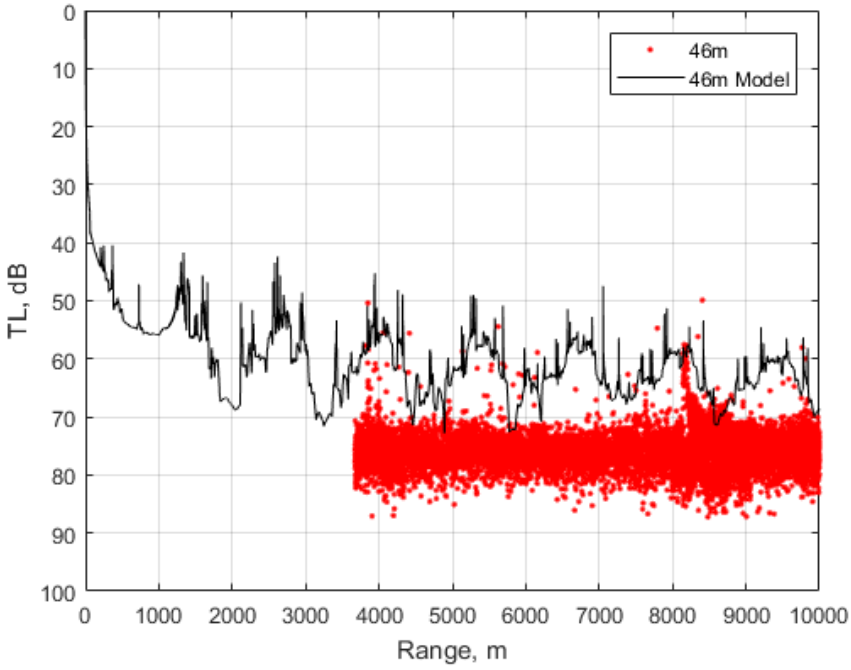

Figure 25. A045 (45m) measured and modeled TL, EMATT at 46m, 950 Hz

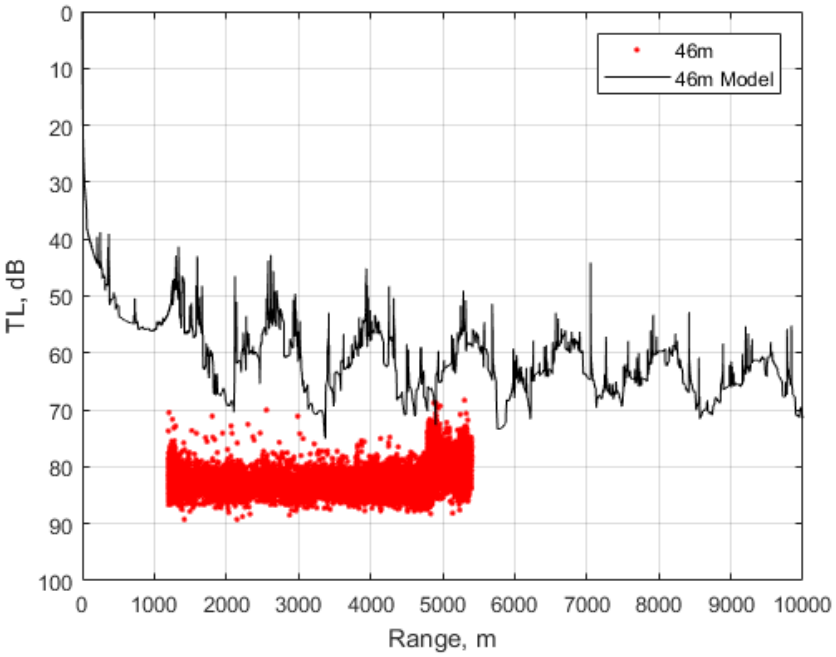

Figure 26. A045 (45m) measured and modeled TL, EMATT at 46m, 2800 Hz

THIS PAGE INTENTIONALLY LEFT BLANK

V. DISCUSSION

A. MEASURED TRANSMISSION LOSS

The measured TL varied widely, even at the same range. The variability at a given range was shown to be up to 30 dB for the 950 Hz signal, and as high as 40 dB for the 2800 Hz signal, as shown in Figures 27 and 28. The general trend of the TL is as expected: there is less TL at close range, and more TL at further ranges. As well, higher variability due to higher frequency is also present, as expected. Taking two different receivers and measuring the TL from the same EMATT results in broadly similar TL results. There are noticeable peaks that only occur on one receiver and not the other (spike at around 5800 m for A020, not present for A023).

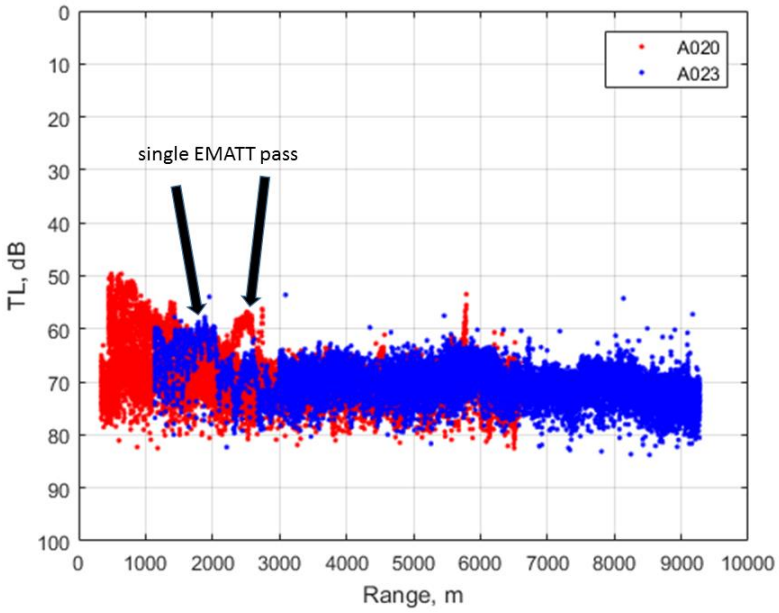

Even at the same range, TL can be variable. The arrows show a single path of the EMATT past the respective receiver.

Figure 27. TL versus range for 183m Acousondes, 950 Hz EMATT at 183m

This suggests that not only range affects TL, but azimuth as well. A large portion of this difference in TL is likely due to the sound speed variability at 50m, as discussed in Chapter IV and demonstrated in Figure 16. As the azimuth to the receiver changes, the

sound propagation is likely travelling through water with slightly different characteristics (including the SSP) and this will cause variations in TL at the receiver, even at the same range.

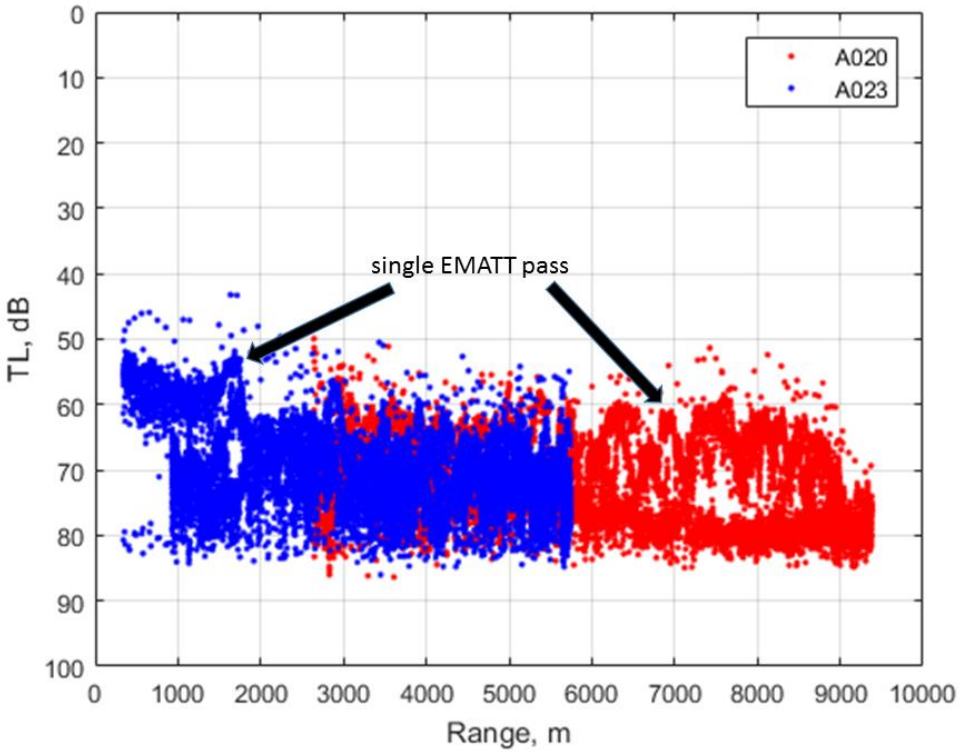

At higher frequencies, the TL shows more variability. The arrows demonstrate areas where there are multiple passes of the Acousonde receiver by the EMATT, each giving different TL.

Figure 28. TL versus range for 183m Acousondes, 2800 Hz EMATT at 183m

The arrows in Figure 27 and 28 highlight a single pass of the EMATT, showing a more favorable acoustic path from that location versus other azimuths at the same range. This occurs at both 950 Hz and 2800 Hz. In Figure 27, we can see two separate paths, one from each EMATT, that have different TL at the same range (approximately 2400 m). This shows that while range is important in determining TL, using a range-independent SSP (i.e., one SSP for an area, regardless of azimuth) for modeling or prediction can lead to over- or underestimating the TL in a very dynamic ocean environment.

B. DIFFERENCES IN TRANSMISSION LOSS BETWEEN MEASURED DATA AND MODELS

There were some significant differences between the measured TL data and the modeled TL. At short range, for the medium and deep EMATT depths (125m and 183m), both the measured and modeled TL followed the same trend: less TL at short ranges, increasing to around 3000m. At this point, the measured TL became generally flat (with large variability) while the modeled TL had very noticeable spikes which indicate convergence of acoustic energy. As well, the measured TL was generally higher than the modeled TL. This can be seen in Figures 29–32. In these figures, TL based on both of the CTDs are plotted, as well as their average (as in Figure 15). This is to show the TL variability from the two separate SSPs that were measured during the 10-hour experiment.

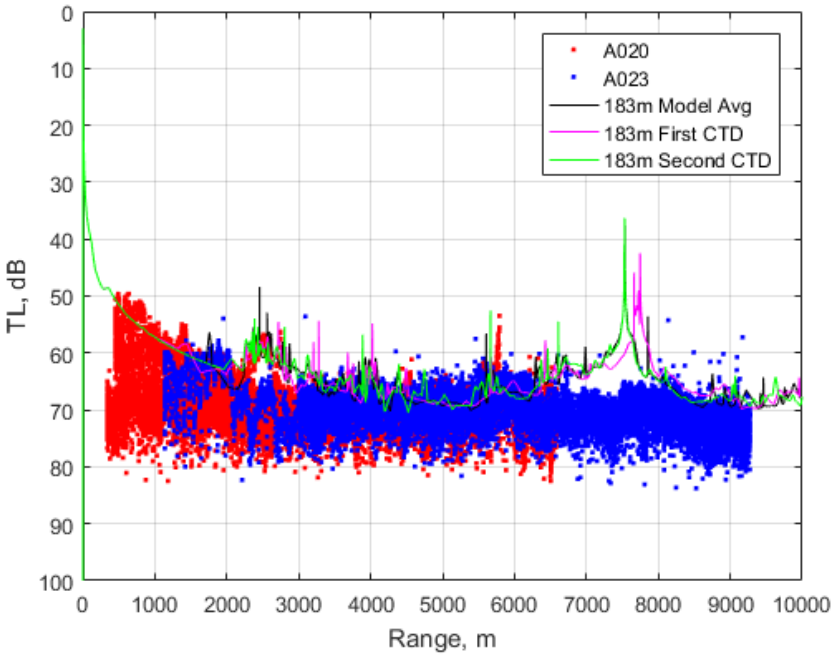

The first area of low TL after 1000 m is at approximately 2300–2700 m. Both the modeled and measured TL follow this trend. Between 4700–5400 m, the modeled TL shows a shadow zone, but the measured TL is actually rather linear. The modeled TL shows a peak in received signal at approximately 7500 m, and this does not show up in the measured TL.

Figure 29. TL versus range for183m Acousondes, EMATT at 183m, 950 Hz

Of specific interest in these figures is that the expected shadow zones shown in the model (i.e., areas of high TL where the acoustic path is not expected to penetrate) are mostly not present in the measured data. The most likely reason for this difference in expected behavior versus measured behavior is twofold. Firstly, there is the presence of surface ice that scatters the acoustic energy, allowing leakage into the shadow zones but also causes higher TL at further range. Secondly, the high variability at around 50m can also affect the acoustic propagation, causing additional scattering. These effects are very prevalent in Figure 32, as at even very short range the TL is much higher than modeled. The strong upward refraction at this layer would cause the energy to be scattered by the surface ice very quickly, and the SSP variability of the layer would result in a highly variable refractive behavior. These effects are magnified when both receiver and transmitter are in this layer.

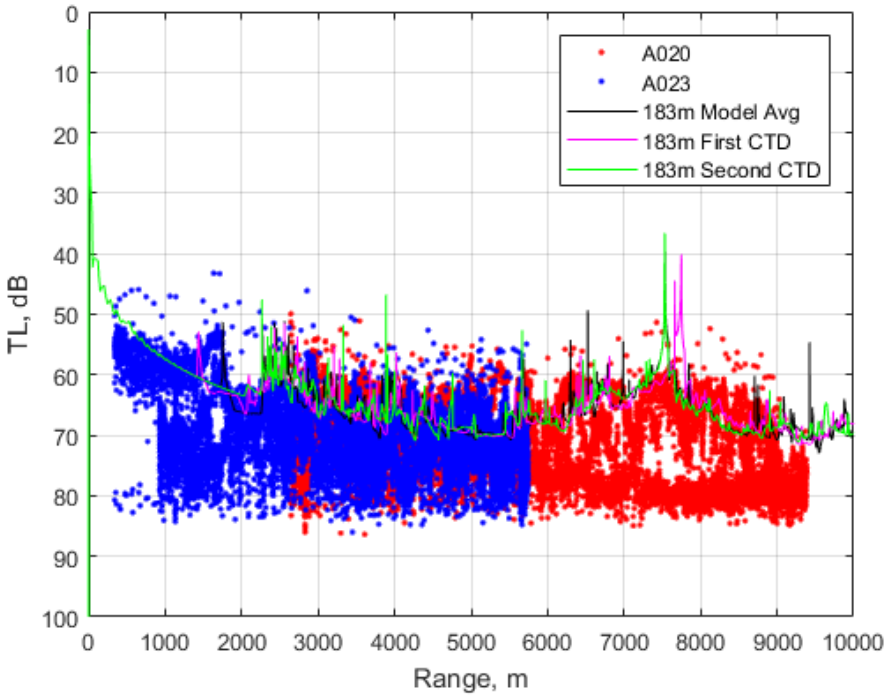

The higher frequency has higher variability, but the general trend of the measured TL follows the modeled TL rather closely, even at further ranges. While the modeled shadow zone at around 5000 m is not present in the measured data, the spikes at 1600 m, 6200 m and even further out at 7500 m can be seen in both modeled and measured data.

Figure 30. TL versus range for183m Acousondes, EMATT at 183m, 2800 Hz

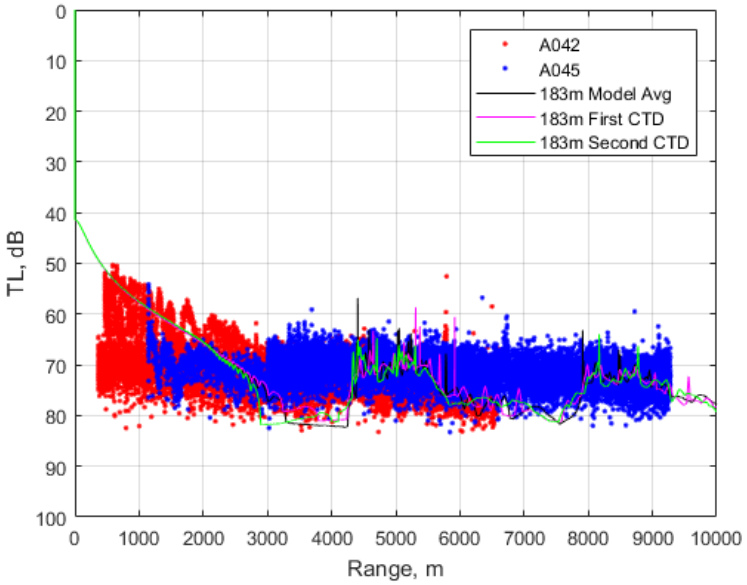

The shadow zones that are present in the modeled data are not present at all in the measured data. For short ranges, the measured TL is less, as is the modeled TL. After about 3000 m, though, the measured becomes flat and does not follow the modeled TL at all.

Figure 31. TL versus range for 45m Acousondes, EMATT at 183m, 950 Hz

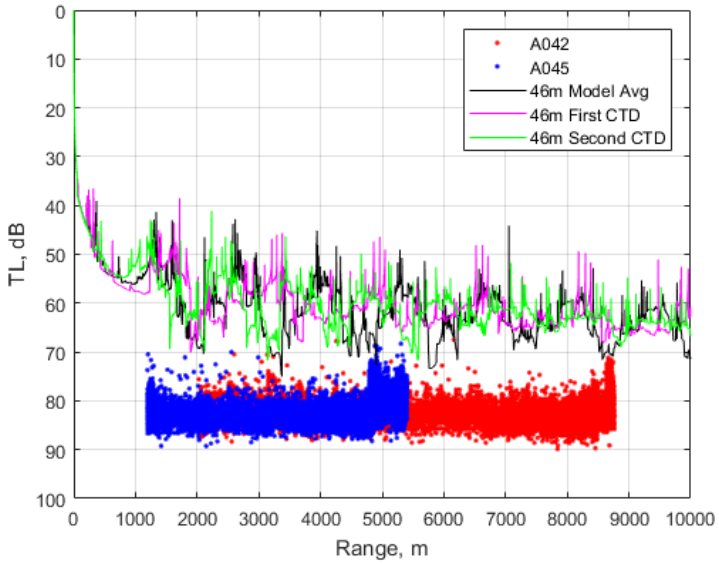

The entirety of the measured TL is very high compared to the modeled TL. In addition, the three modeled TLs (based on the different SSPs) show that the variation over just the 10-hour experiment causes extremely different acoustic paths and highly variable TL.

Figure 32. TL versus range for 45m Acousondes, EMATT at 46m, 950 Hz

THIS PAGE INTENTIONALLY LEFT BLANK

VI. CONCLUSION

A. SUMMARY

Two EMATTs were deployed under Arctic ice cover in order to study short range acoustic propagation. Two separate SSPs were obtained, one before and one after EMATT deployment, in order to model the expected TL in this environment. Two VLAs and a single Acousonde receiver were placed in the water to record the EMATTs' acoustic emissions. This received level was used to calculate the TL for the acoustic path between the EMATTs and the Acousonde receivers, plotted as TL versus range.

The conclusion from this experiment is that both surface ice cover and the presence of a highly variable layer at approximately 50 m caused highly variable TL at all tested depths. Though the model was relatively accurate over very short ranges (under 2000 m) for medium and deep EMATT depths, as ranges increased between EMATT and Acousonde, the modeled TL and the measured TL began to differ widely. This is because the model does not capture any of the temperature variability; it can only run static temperature models. The model also cannot accurately represent surface ice interaction with the acoustic energy.

B. TACTICAL IMPLICATIONS

The presence of the highly variable 50 m layer, as well as the presence of a near-surface temperature maximum, are not present in the GDEM data. This presents an obvious problem for units working in this region if they are unable to have accurate SSP data to plan their operations. While measuring the SSP using normal bathymetric equipment is possible, tactical considerations such as emitted noise and emissions control restrictions could restrict units from receiving updated climatological data from satellites. This does not even consider the difficulty in under-ice transits by submarines, where they may be out of satellite communications for long periods of time. An accurate picture of the undersea environment is critical in order to exploit it tactically, both offensively and defensively.

C. FUTURE WORK AND RECOMMENDATIONS

The difficulty in ascertaining an accurate EMATT location after initial CPA of VLA 1 and 2 likely contributed to some of the differences between measured and modeled TL. Future work could include researching methods to extract orientation and location data from slices of a spectrogram; in this case, using the 15-minute legs to determine where the EMATT is relative to the Acousonde. Fitting the recorded data to a series of theoretical spectrogram curves would allow estimation of simulated CPA, resulting in the orientation of the EMATT, providing much more accurate positional information.

A recommendation for future ICEX experiments would be to have the EMATT transit in a ladder-type pattern, as shown in Figure 33. This would allow for accurate CPA calculations on each leg, versus the single CPA calculation for this experiment. As well, offsetting the EMATTs and Acousondes both by 90 degrees would allow for a drift comparison, which would allow a current estimate from their location data. Measuring the current through the water column would also assist in EMATT localization.

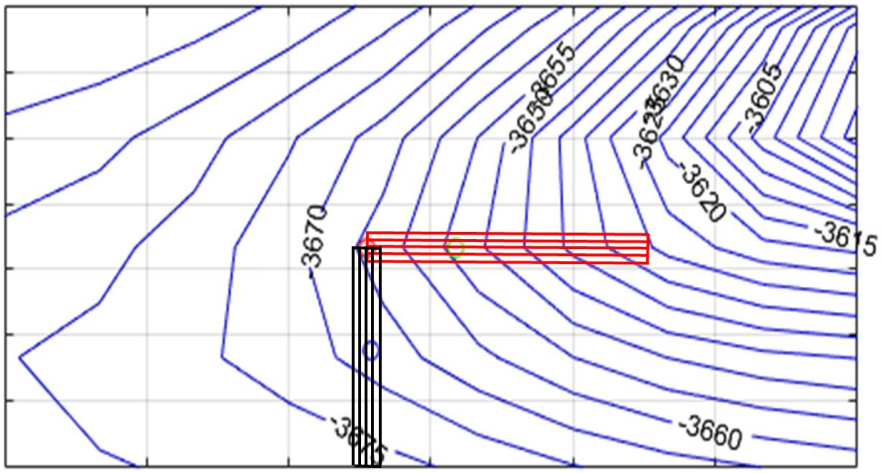

Figure 33. Recommended orientation of EMATT tracks and VLA positions for future ICEX experiments

APPENDIX A. ACOUSONDE SPECTROGRAM FIGURES

A. 10 MARCH

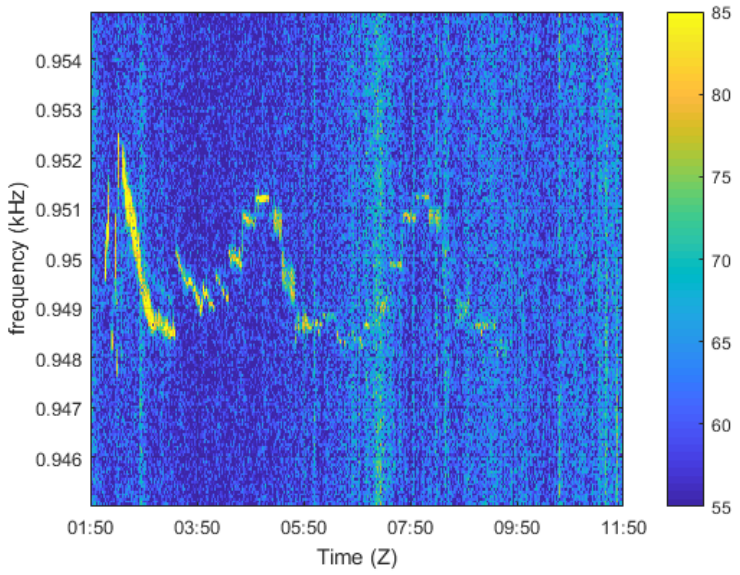

Figure 34. 10 Mar spectrogram from Acousonde A020 for EMATT 1, 950 Hz

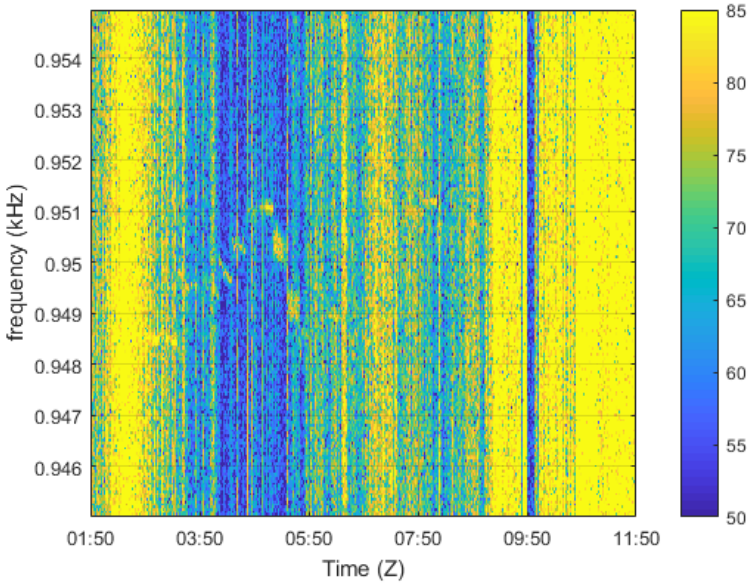

Figure 35. 10 Mar spectrogram from Acousonde A023 for EMATT 1, 950 Hz

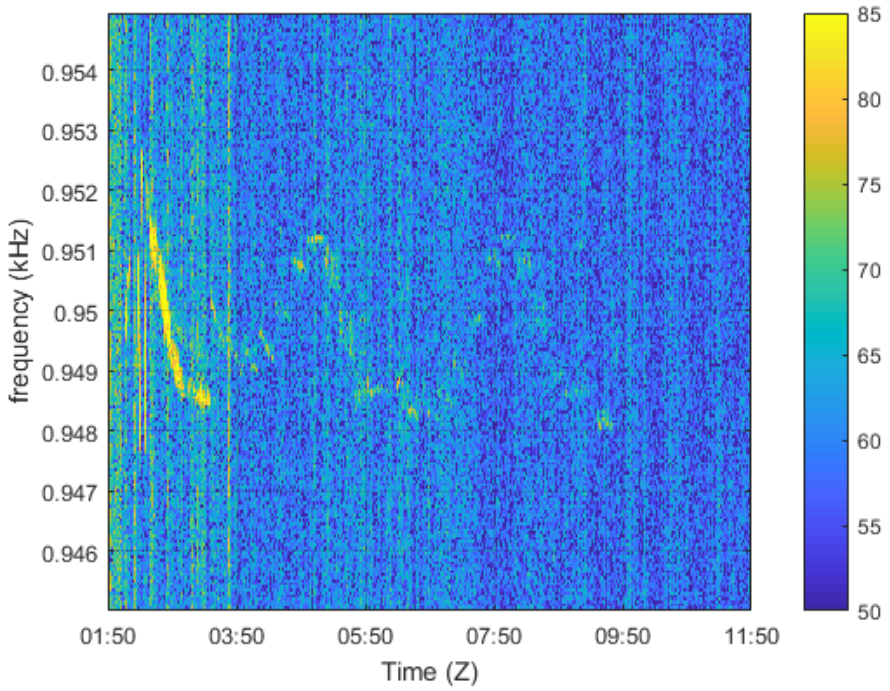

Figure 36. 10 Mar spectrogram from Acousonde A042 for EMATT 1, 950 Hz

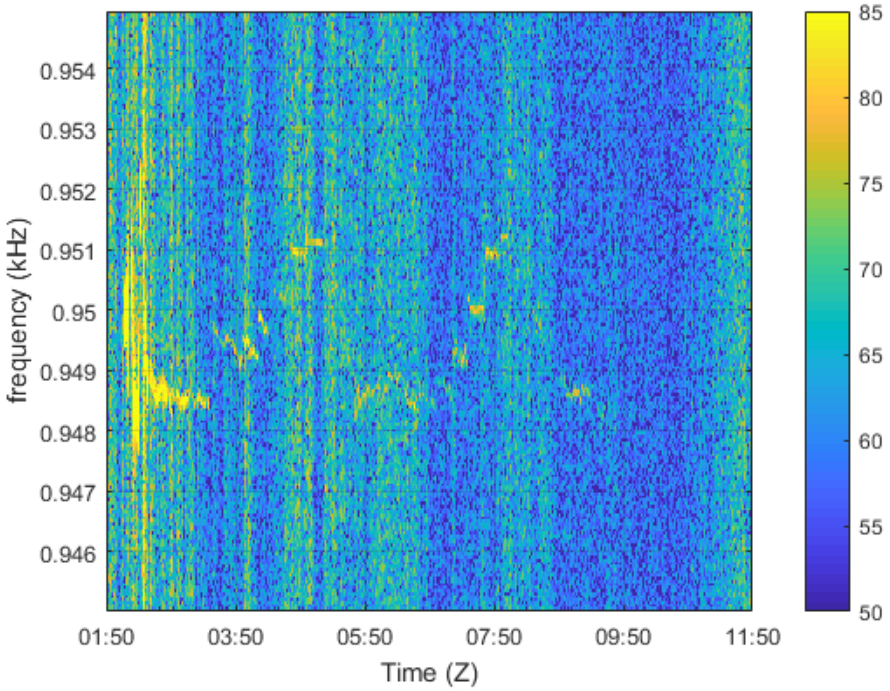

Figure 37. 10 Mar spectrogram from Acousonde A044 for EMATT 1, 950 Hz

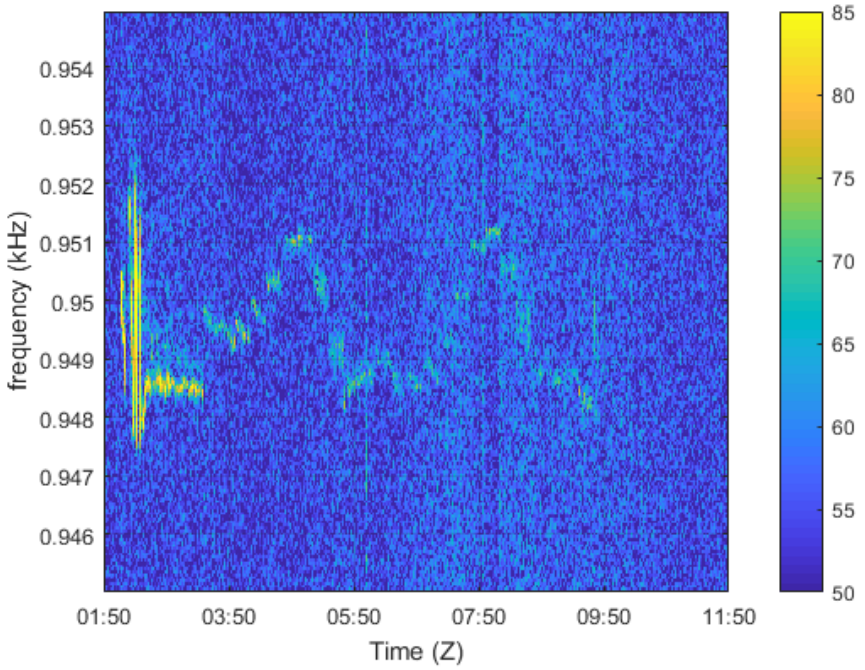

Figure 38. 10 Mar spectrogram from Acousonde A045 for EMATT 1, 950 Hz

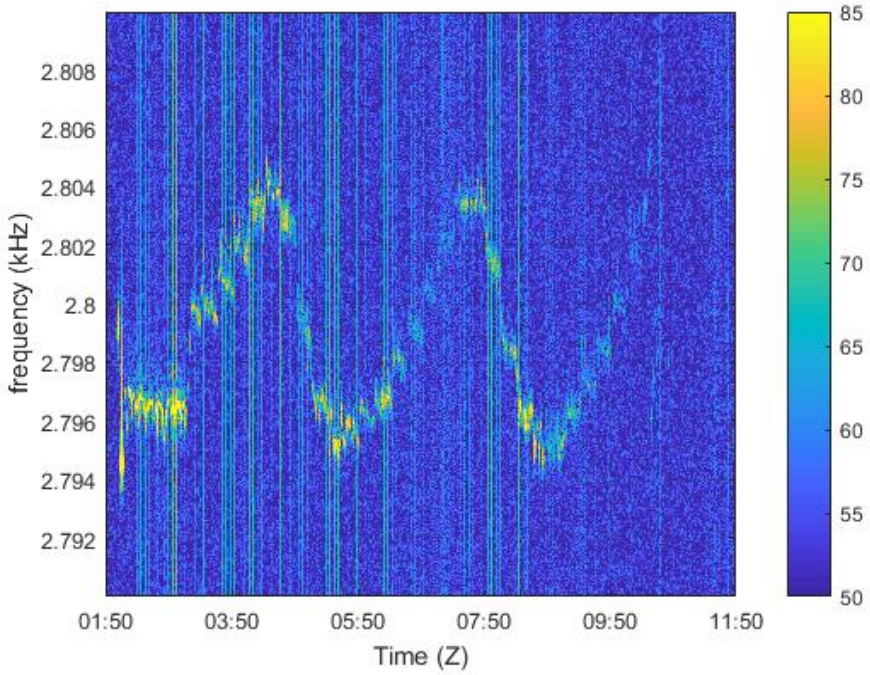

Figure 39. 10 Mar spectrogram from Acousonde A020 for EMATT 2, 2800 Hz

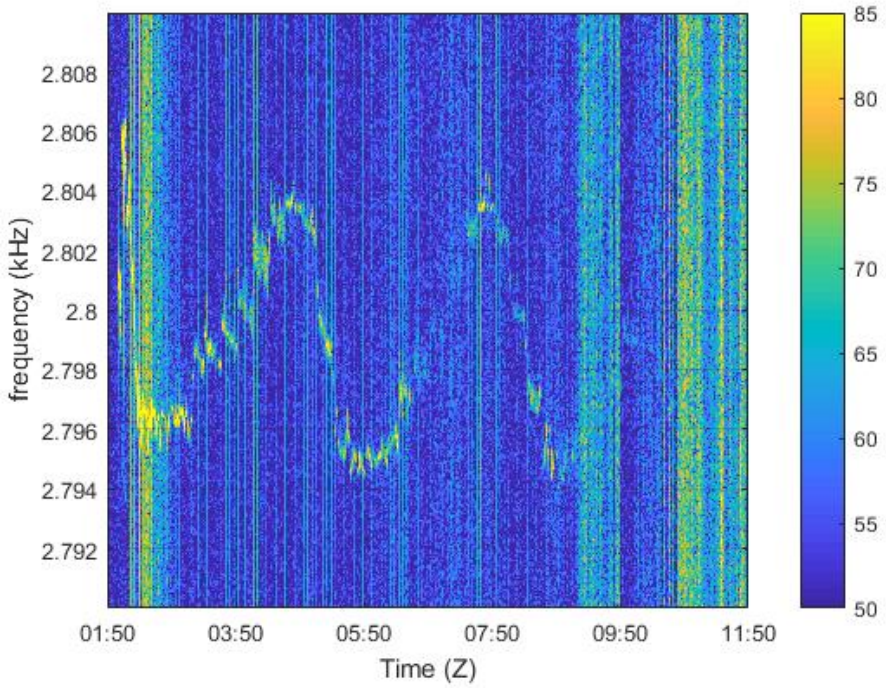

Figure 40. 10 Mar spectrogram from Acousonde A023 for EMATT 2, 2800 Hz

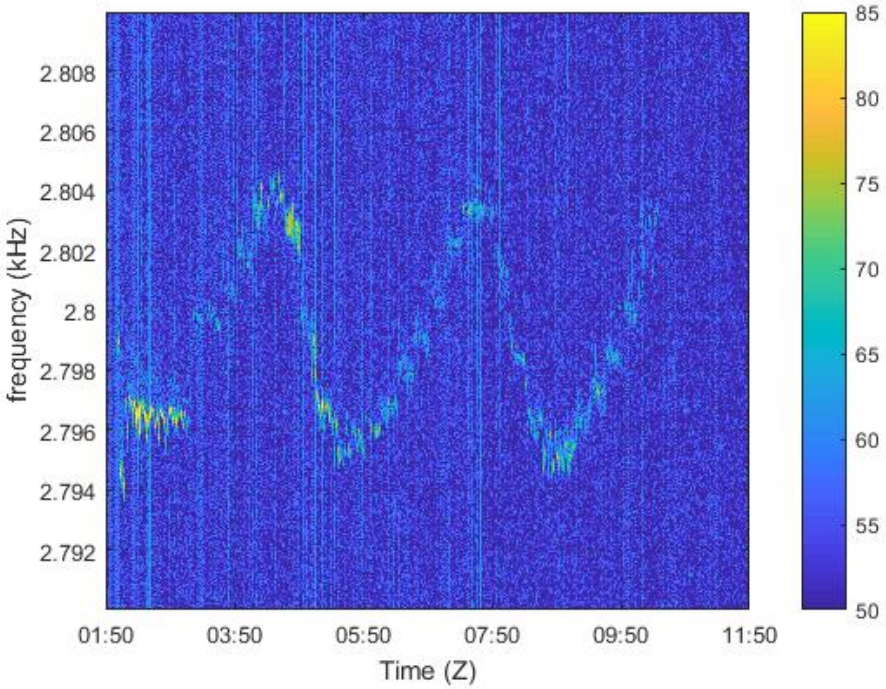

Figure 41. 10 Mar spectrogram from Acousonde A042 for EMATT 2, 2800 Hz

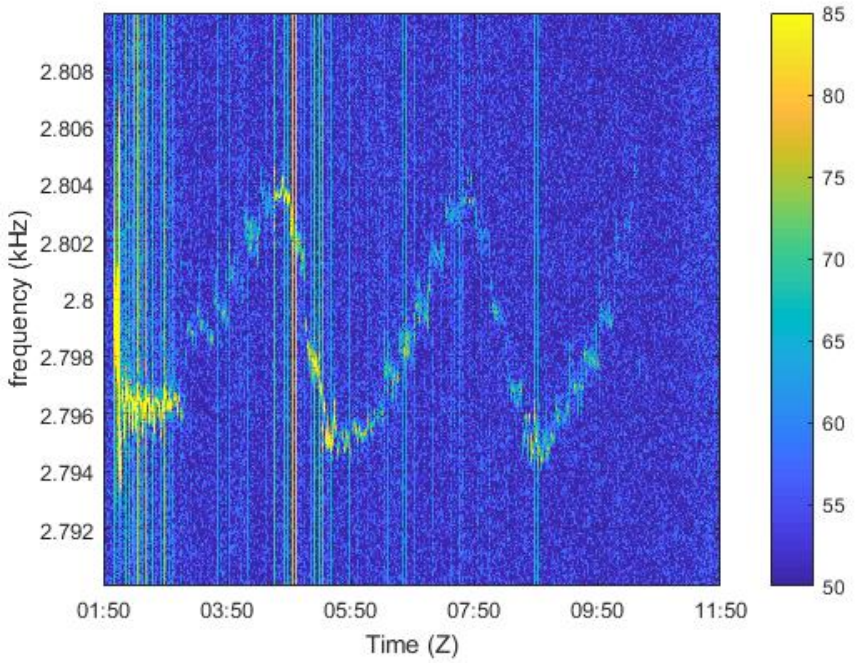

Figure 42. 10 Mar spectrogram from Acousonde A044 for EMATT 2, 2800 Hz

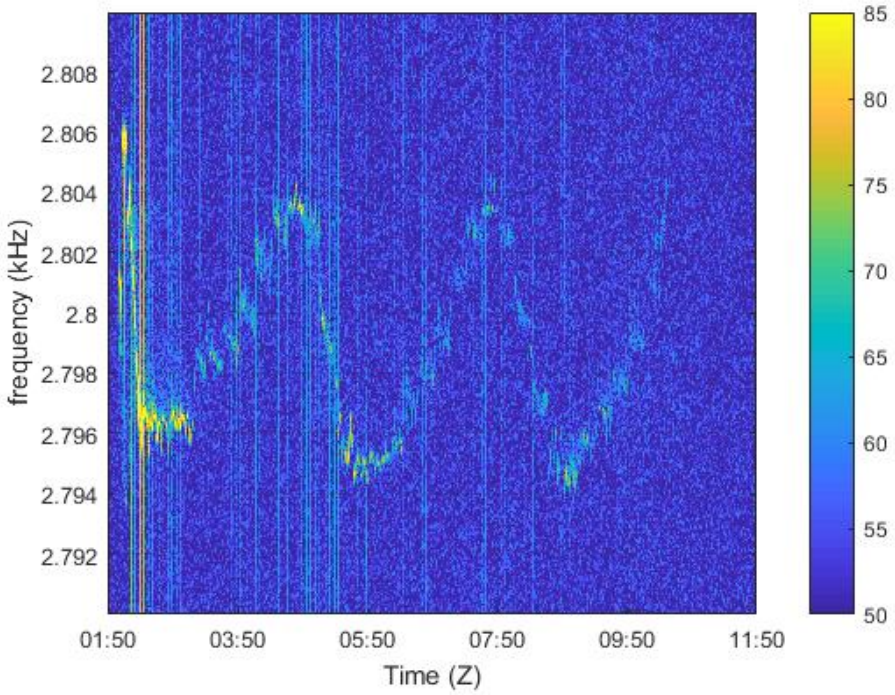

Figure 43. 10 Mar spectrogram from Acousonde A045 for EMATT 2, 2800 Hz

B. 12 MARCH

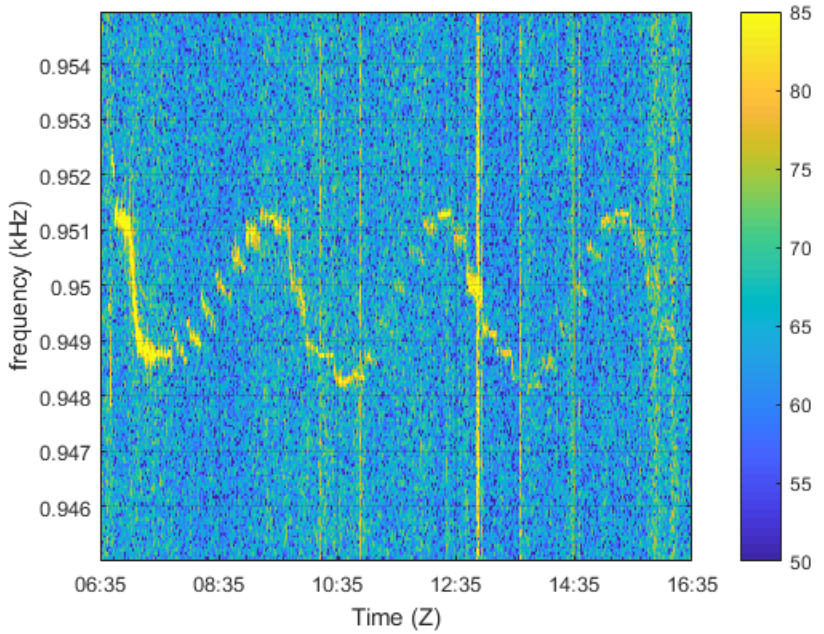

Figure 44. 12 Mar spectrogram from Acousonde A020 for EMATT 1, 950 Hz

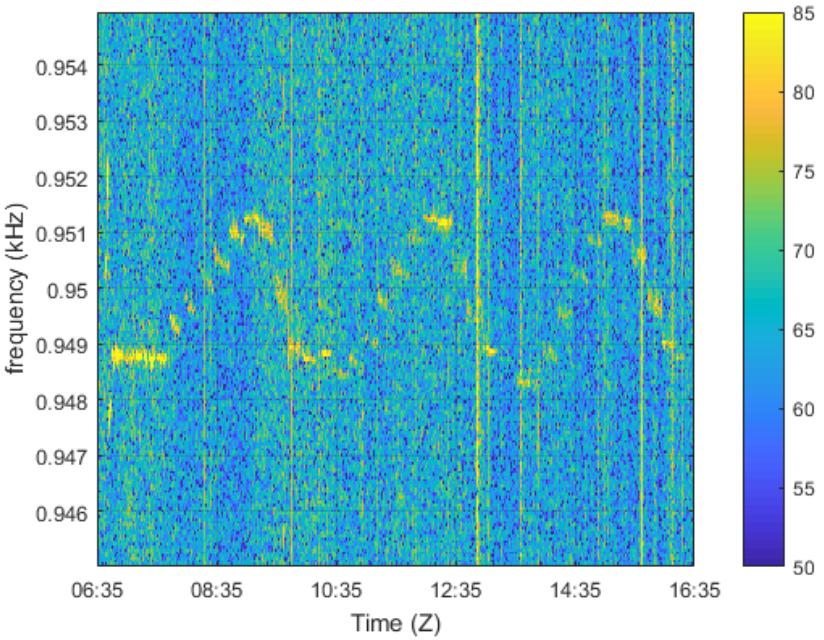

Figure 45. 12 Mar spectrogram from Acousonde A023 for EMATT 1, 950 Hz

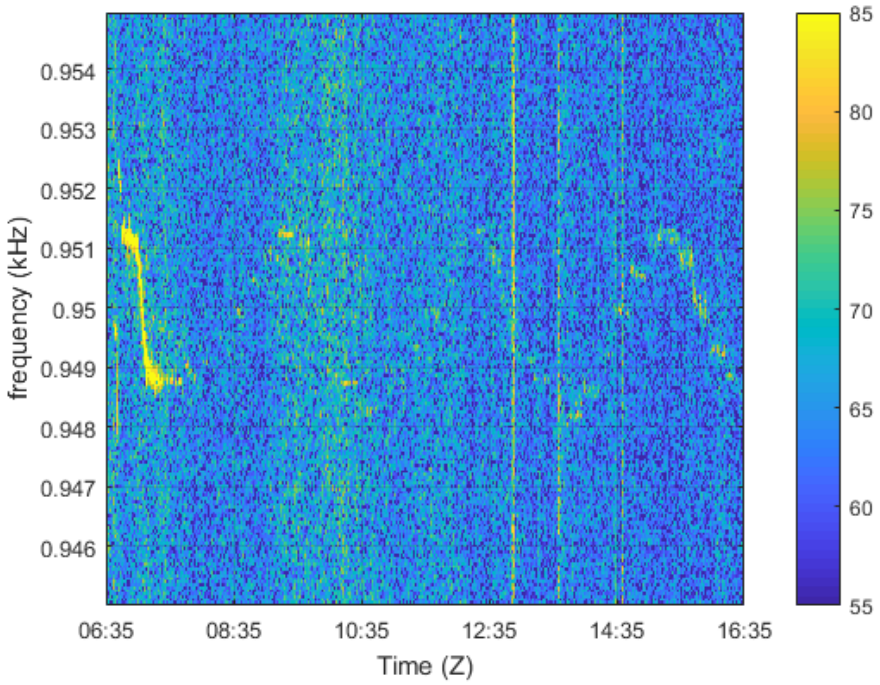

Figure 46. 12 Mar spectrogram from Acousonde A042 for EMATT 1, 950 Hz

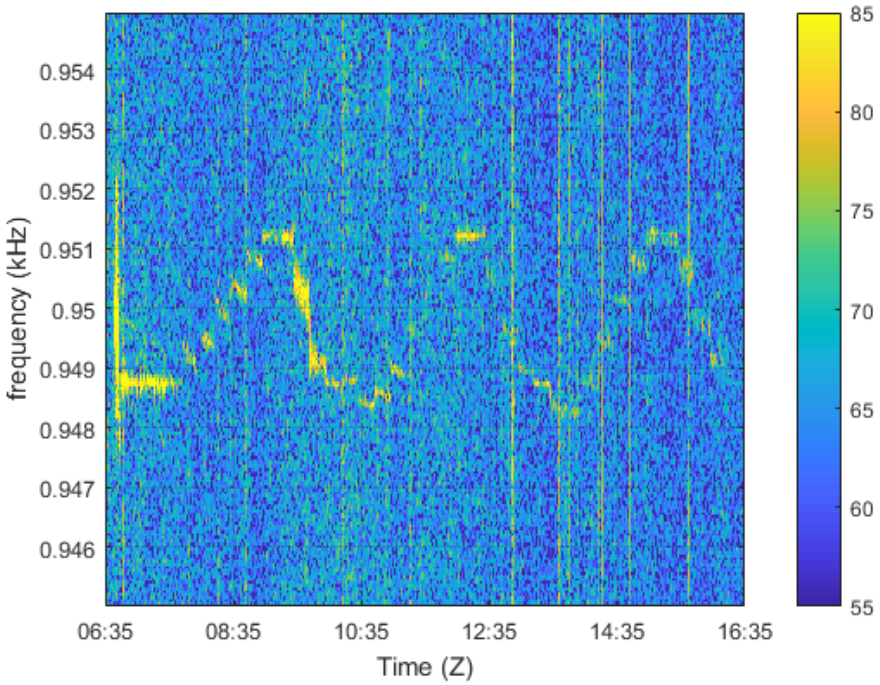

Figure 47. 12 Mar spectrogram from Acousonde A044 for EMATT 1, 950 Hz

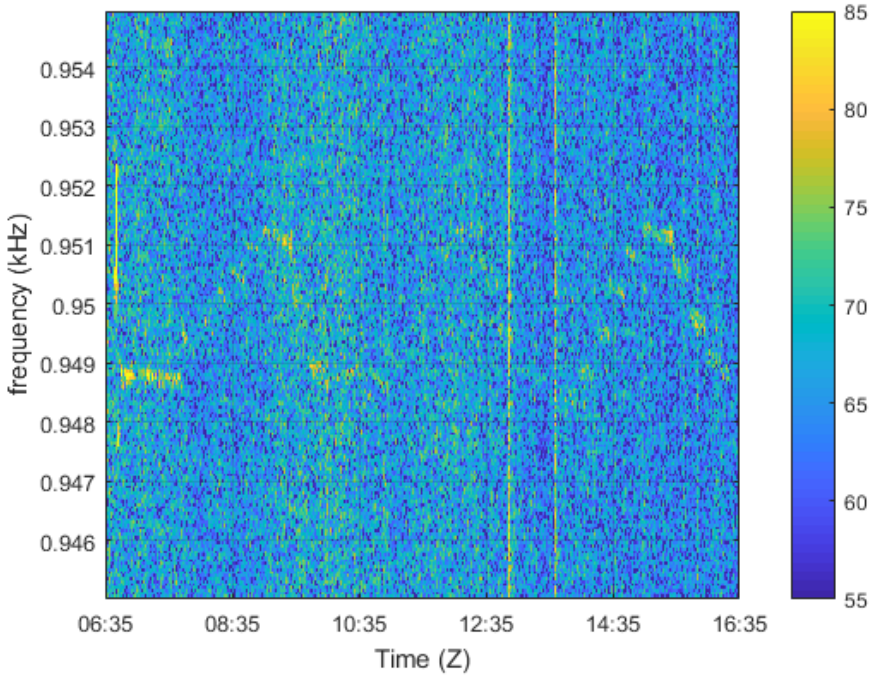

Figure 48. 12 Mar spectrogram from Acousonde A045 for EMATT 1, 950 Hz

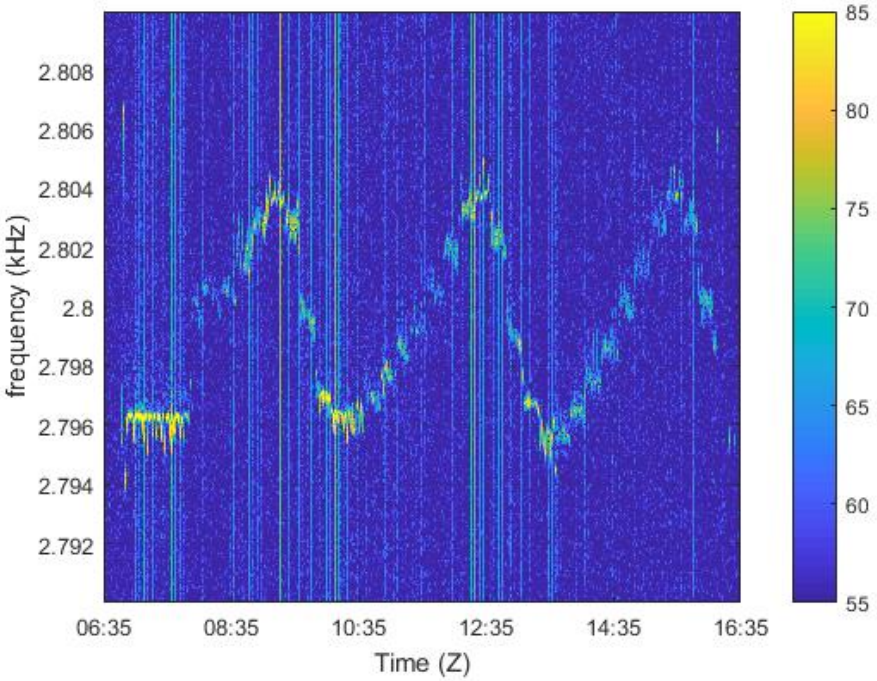

Figure 49. 12 Mar spectrogram from Acousonde A020 for EMATT 2, 2800 Hz

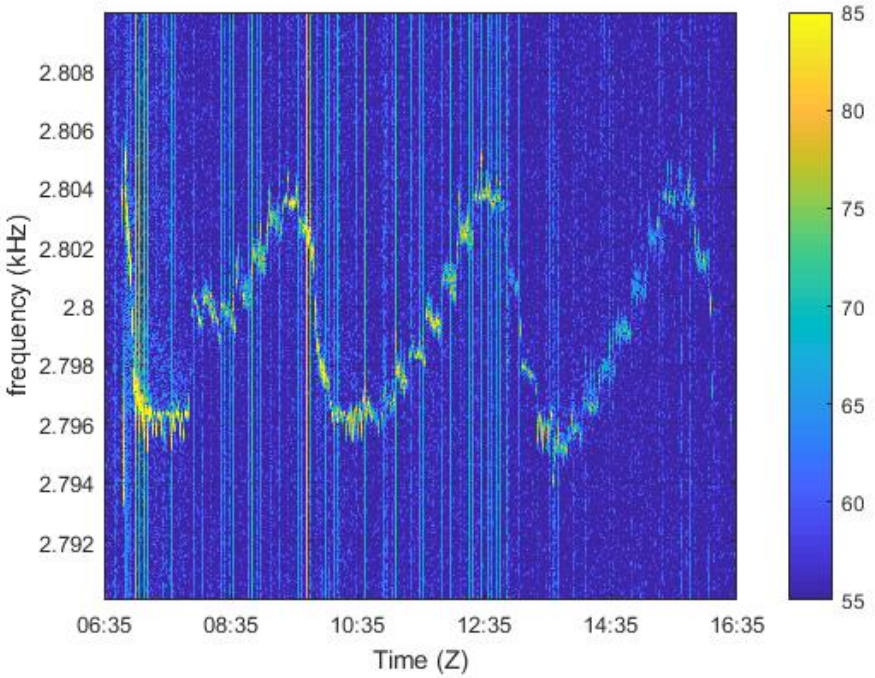

Figure 50. 12 Mar spectrogram from Acousonde A023 for EMATT 2, 2800 Hz

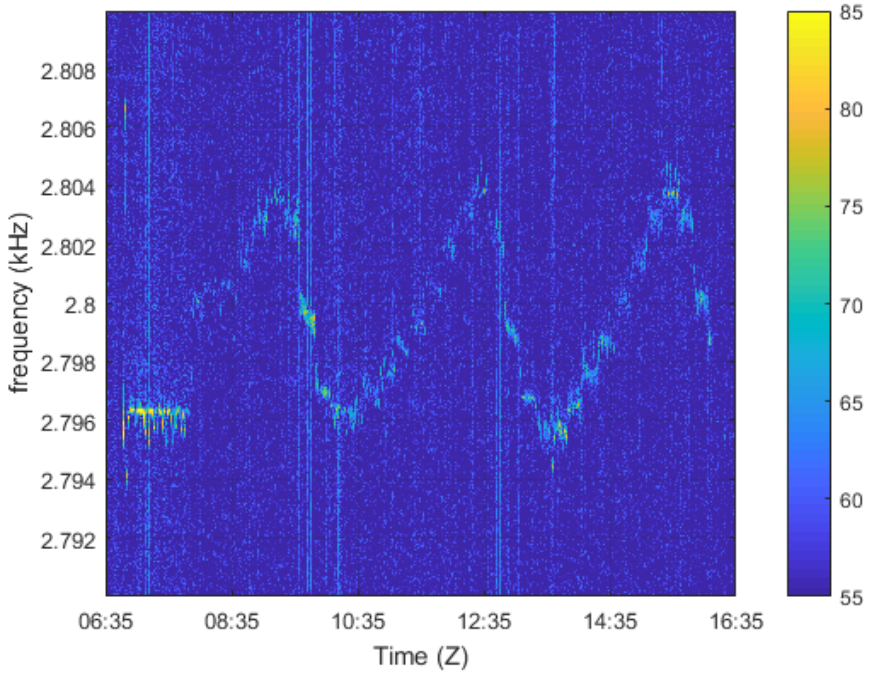

Figure 51. 12 Mar spectrogram from Acousonde A042 for EMATT 2, 2800 Hz

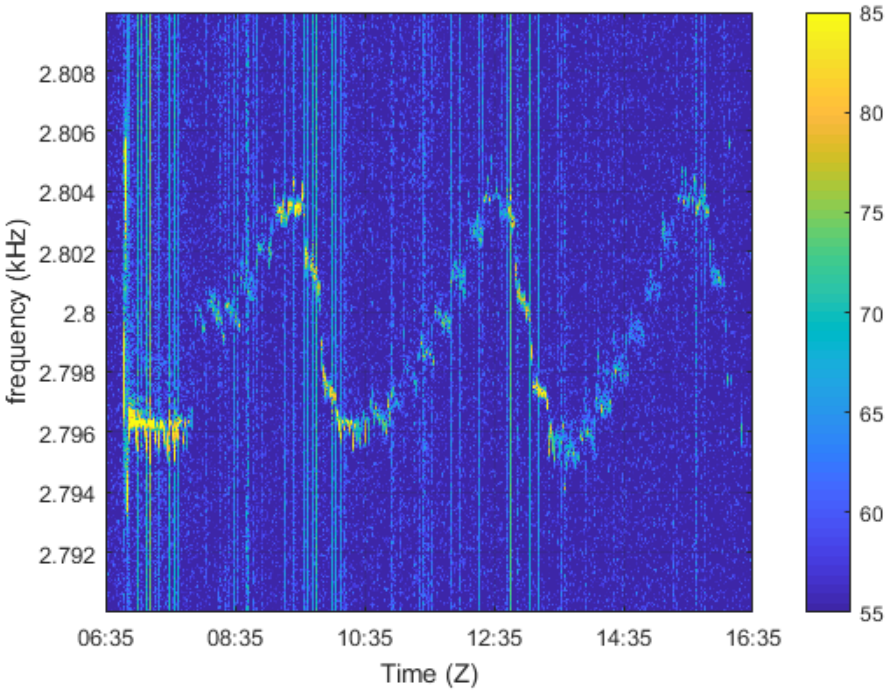

Figure 52. 12 Mar spectrogram from Acousonde A044 for EMATT 2, 2800 Hz

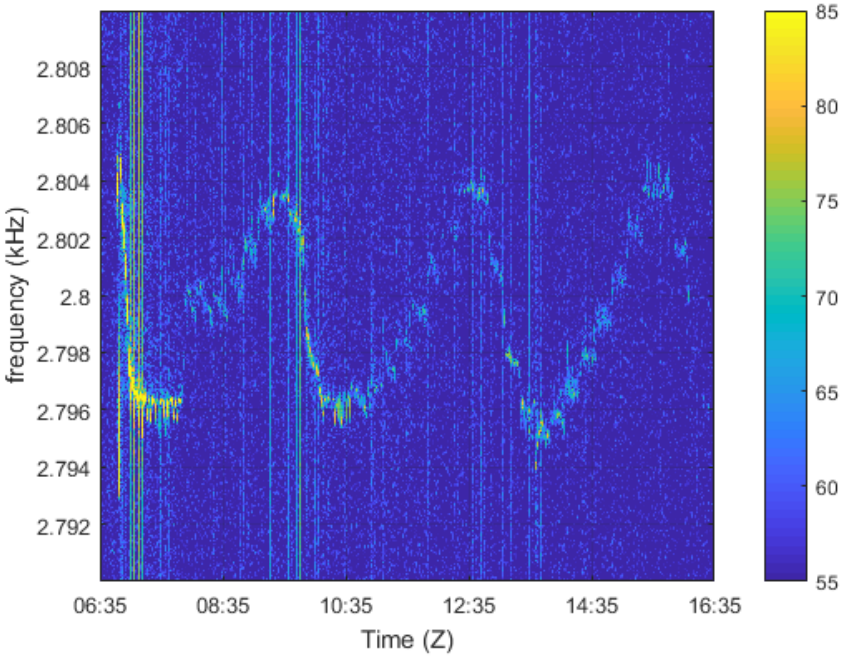

Figure 53. 12 Mar spectrogram from Acousonde A045 for EMATT 2, 2800 Hz

APPENDIX B. MODELED TRANSMISSION LOSS FIGURES

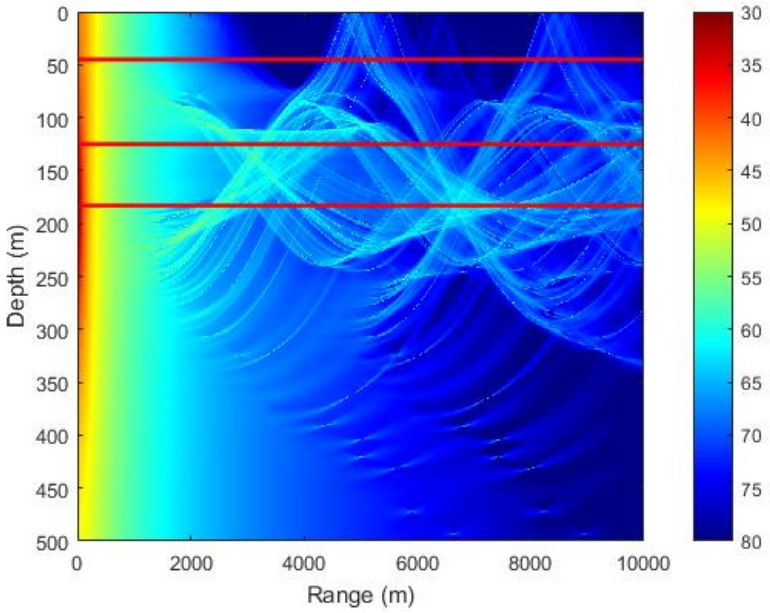

Figure 54. Modeled 950 Hz TL with EMATT at 46m

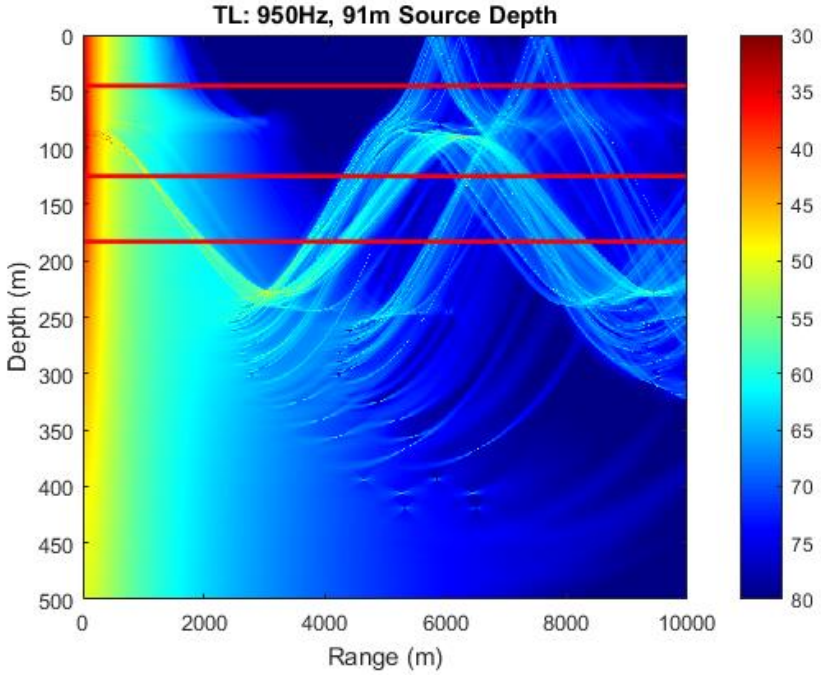

Figure 55. Modeled 950 Hz TL with EMATT at 91m

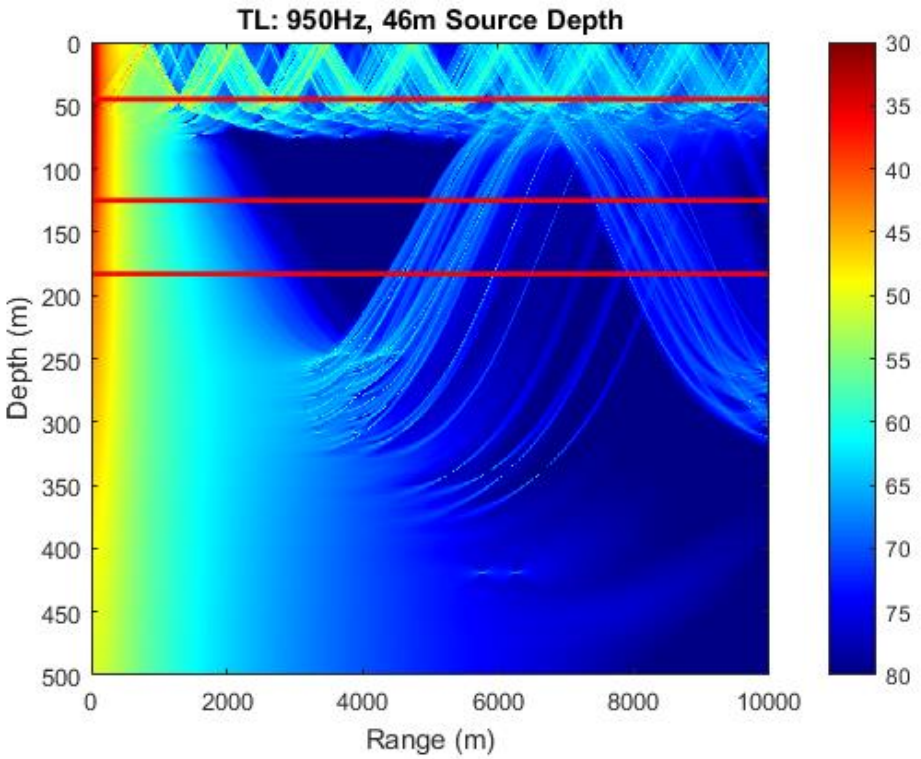

Figure 56. Modeled 2800 Hz TL with EMATT at 183m

APPENDIX C. MEASURED AND MODELED TRANSMISSION LOSS FIGURES

A. EMATT 1, 950 HZ

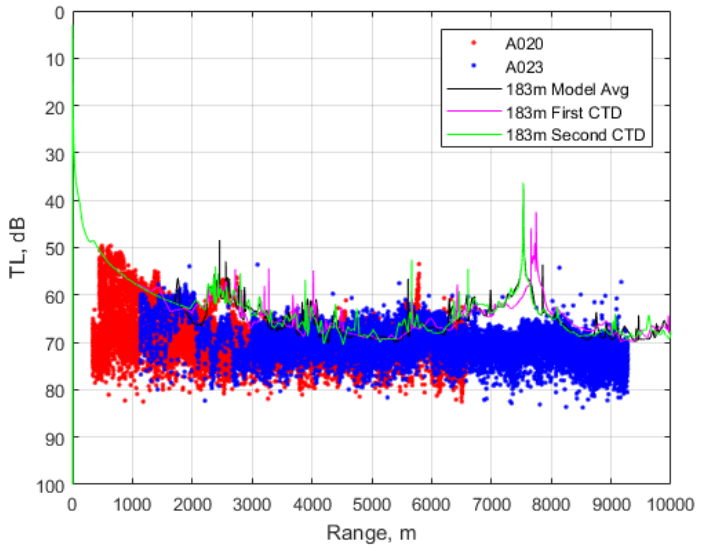

Figure 57. 183m Acousondes (A020, A023), EMATT at 183m, 950 Hz

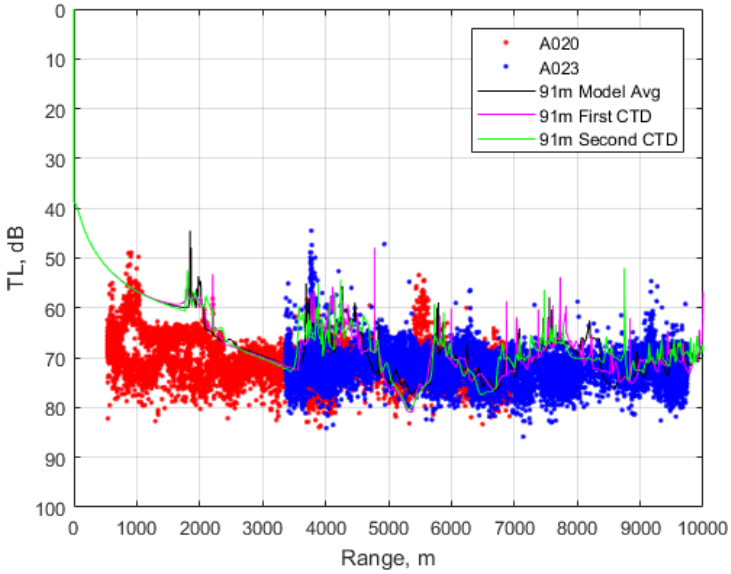

Figure 58. 183m Acousondes (A020, A023), EMATT at 91m, 950 Hz

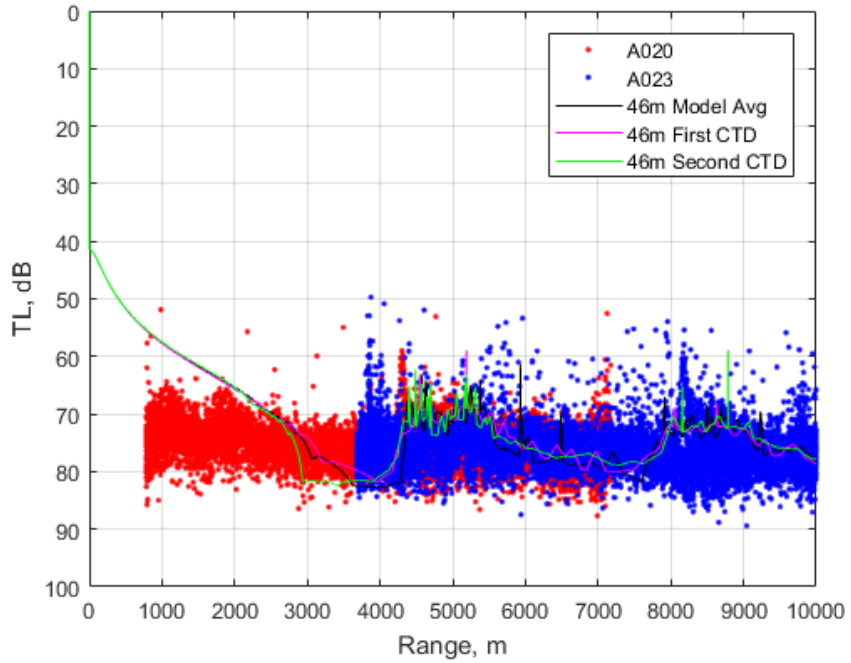

Figure 59. 183m Acousondes (A020, A023), EMATT at 46m, 950 Hz

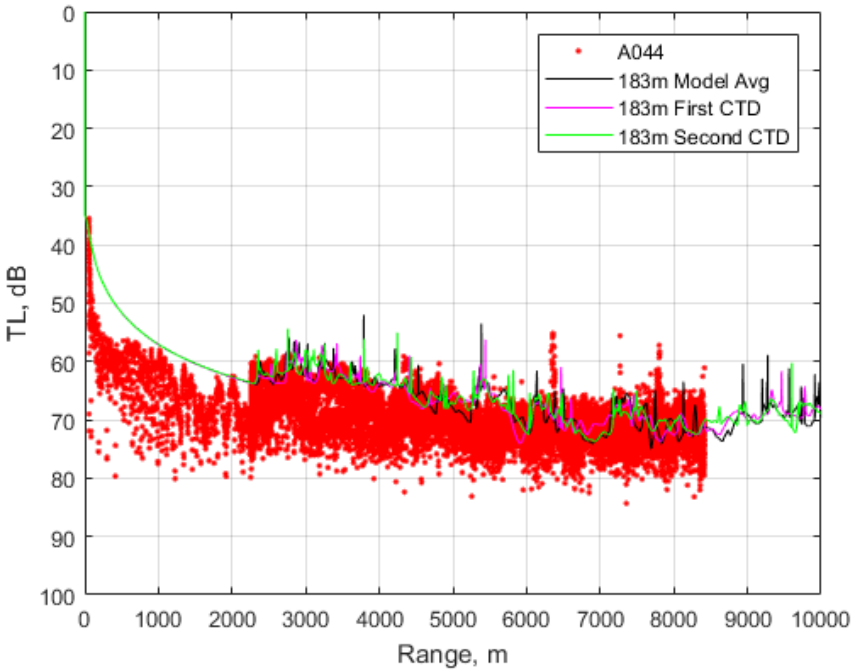

Figure 60. 125m Acousonde (A044), EMATT at 183m, 950 Hz

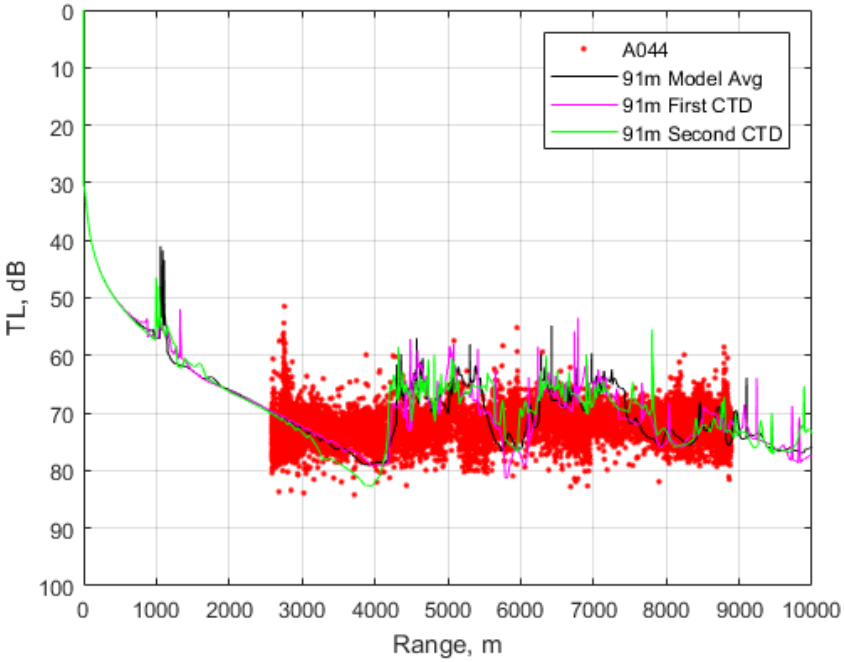

Figure 61. 125m Acousonde (A044), EMATT at 91m, 950 Hz

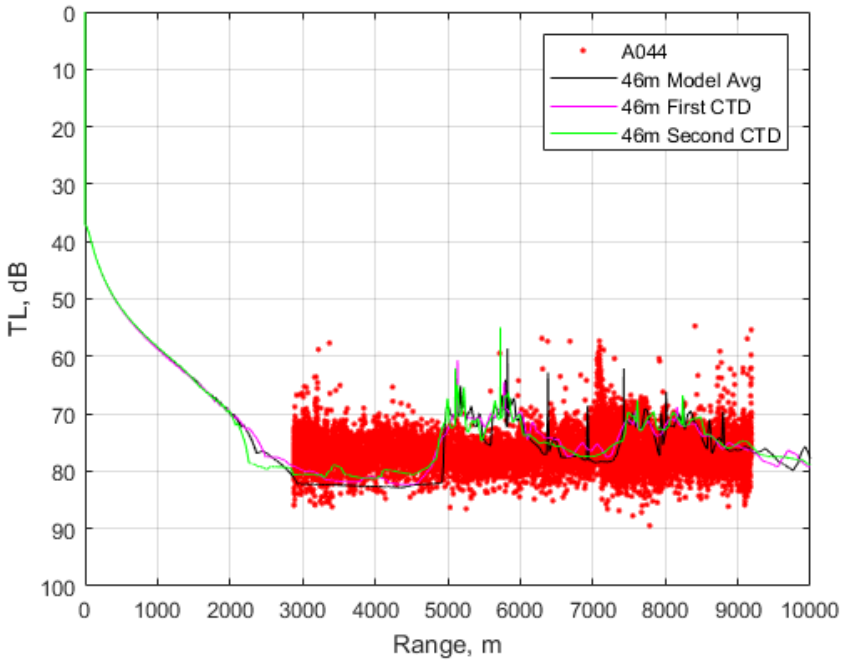

Figure 62. 125m Acousonde (A044), EMATT at 46m, 950 Hz

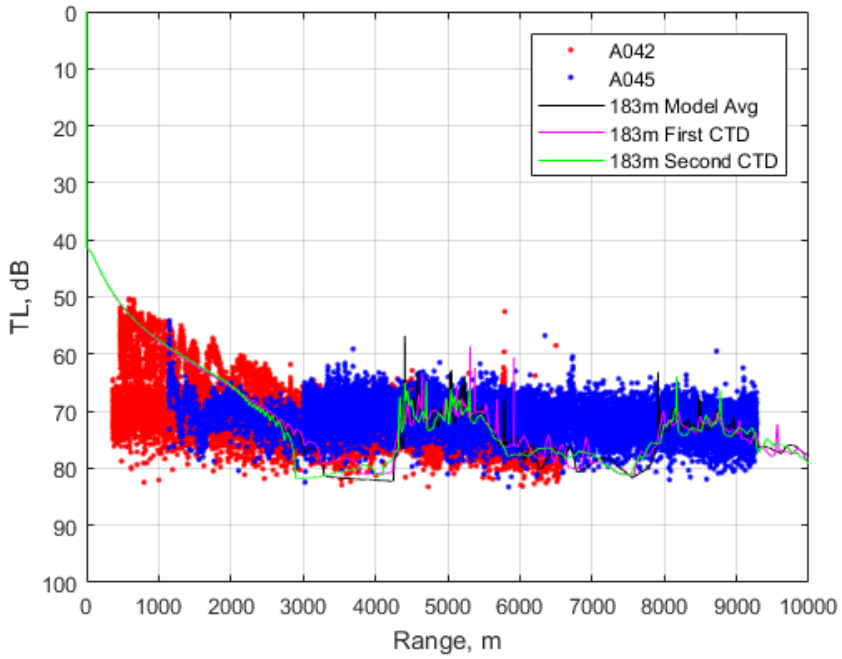

Figure 63. 45m Acousondes (A042, A045), EMATT at 183m, 950 Hz

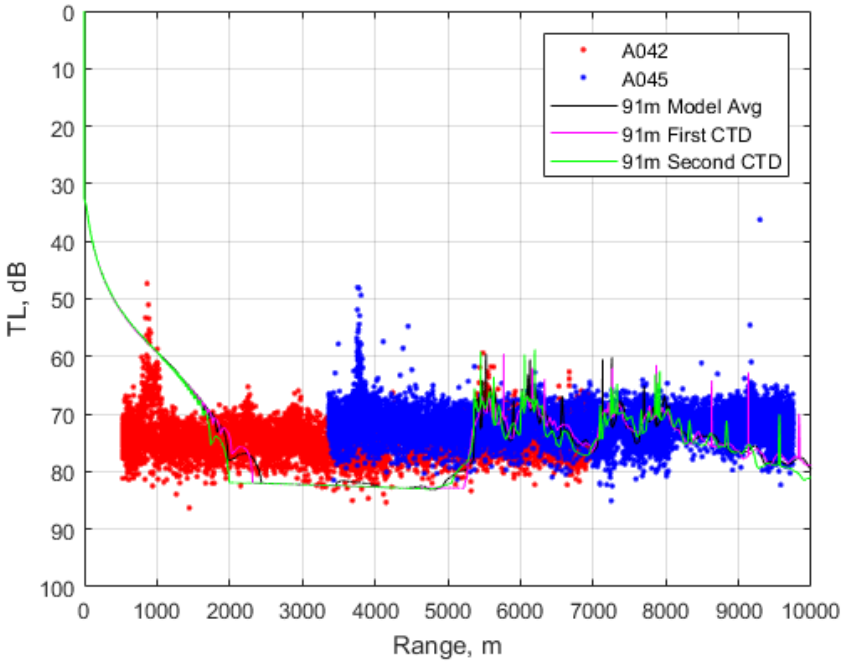

Figure 64. 45m Acousondes (A042, A045), EMATT at 91m, 950 Hz

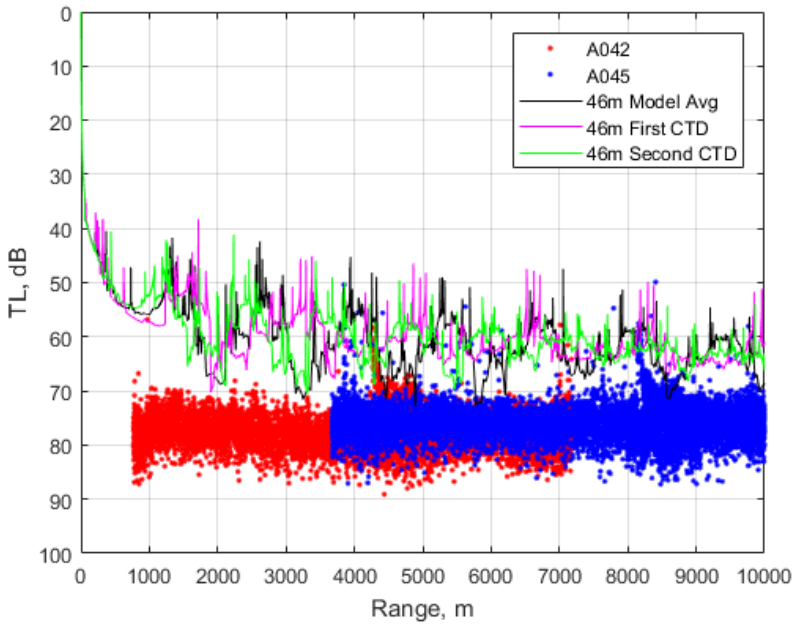

Figure 65. 45m Acousondes (A042, A045), EMATT at 46m, 950 Hz

B. EMATT 2, 2800 HZ

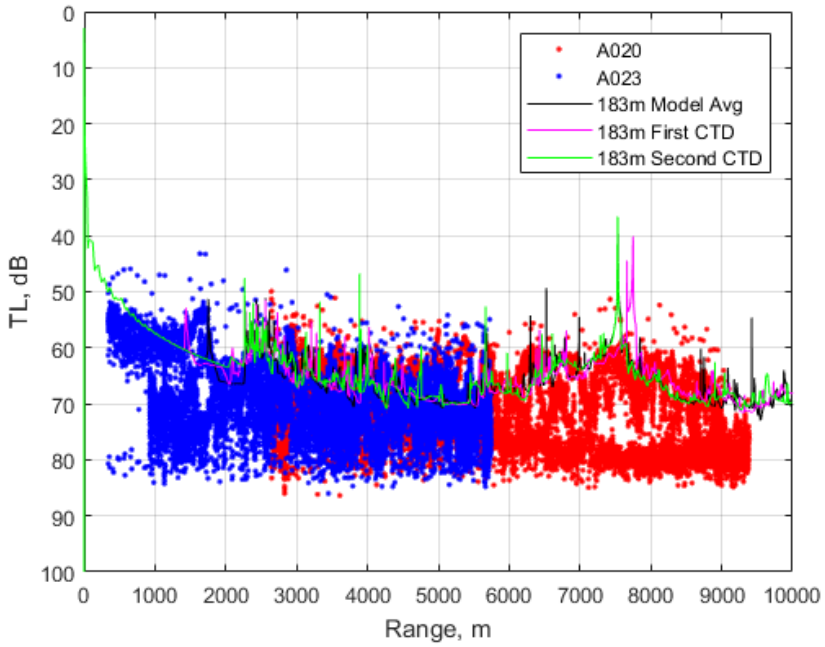

Figure 66. 183m Acousondes (A020, A023), EMATT at 183m, 2800 Hz

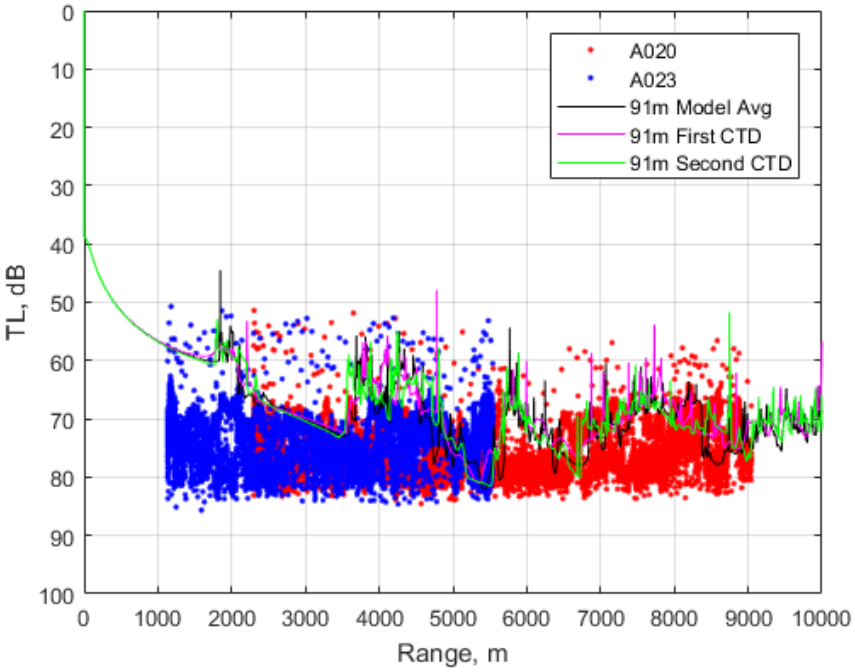

Figure 67. 183m Acousondes (A020, A023), EMATT at 91m, 2800 Hz

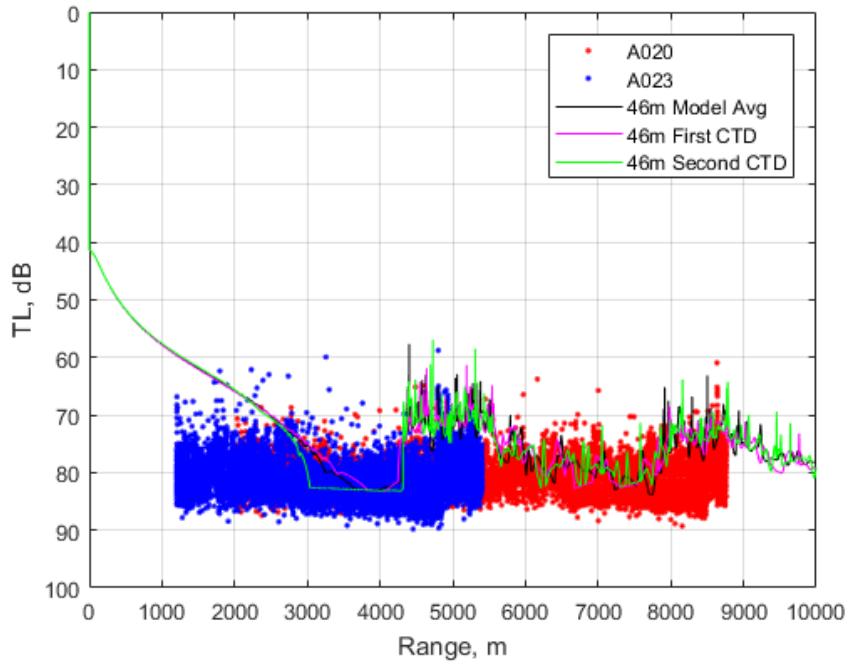

Figure 68. 183m Acousondes (A020, A023), EMATT at 46m, 2800 Hz

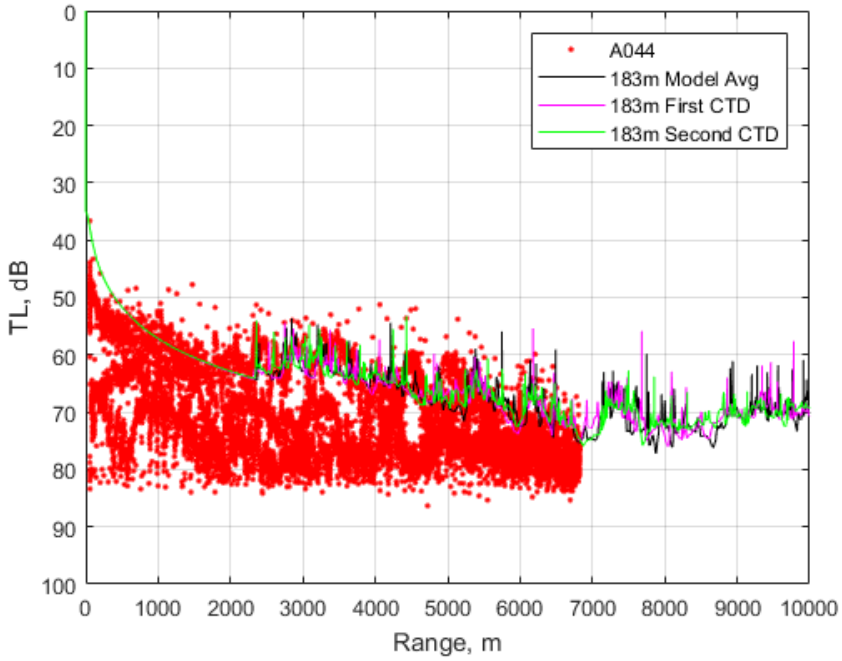

Figure 69. 125m Acousonde (A044), EMATT at 183m, 2800 Hz

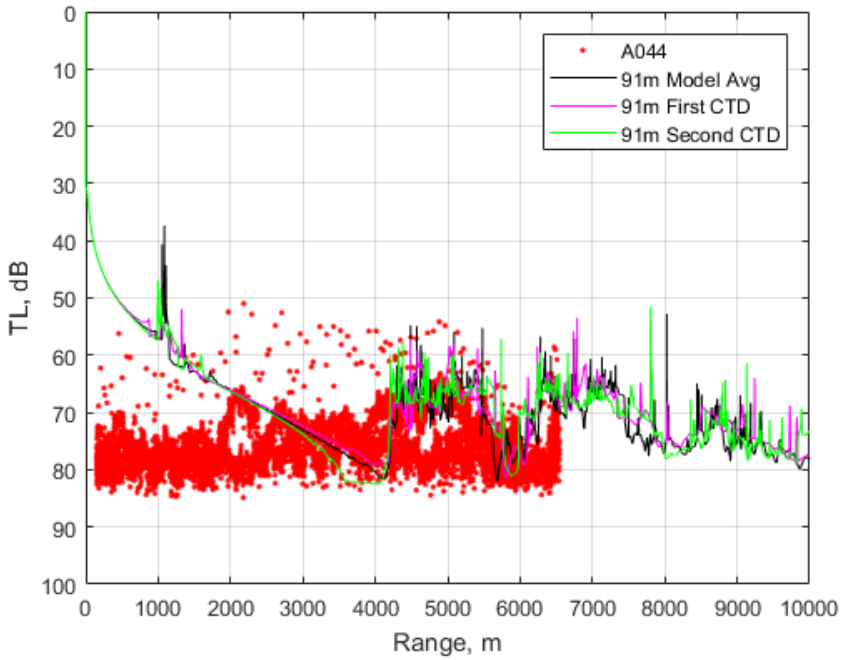

Figure 70. 125m Acousonde (A044), EMATT at 91m, 2800 Hz

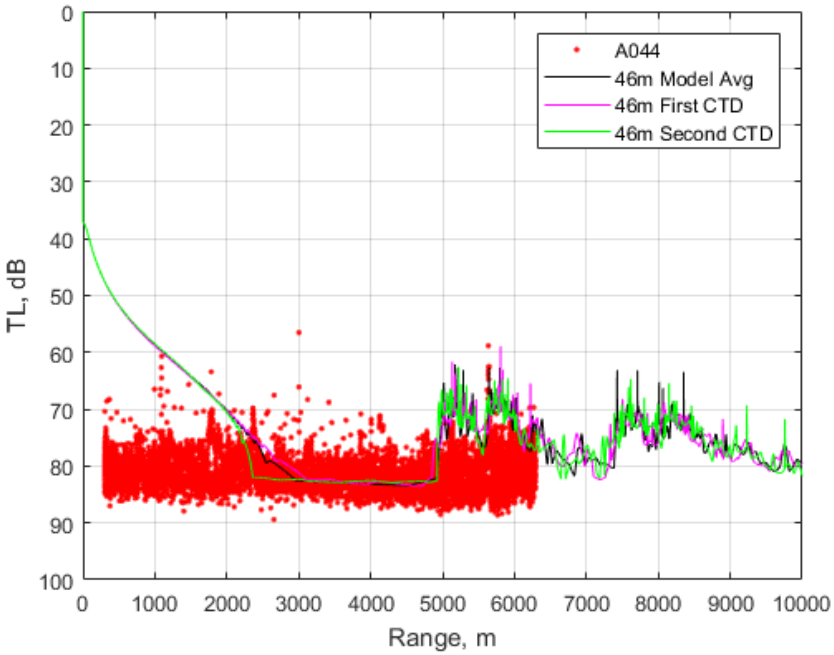

Figure 71. 125m Acousonde (A044), EMATT at 46m, 2800 Hz

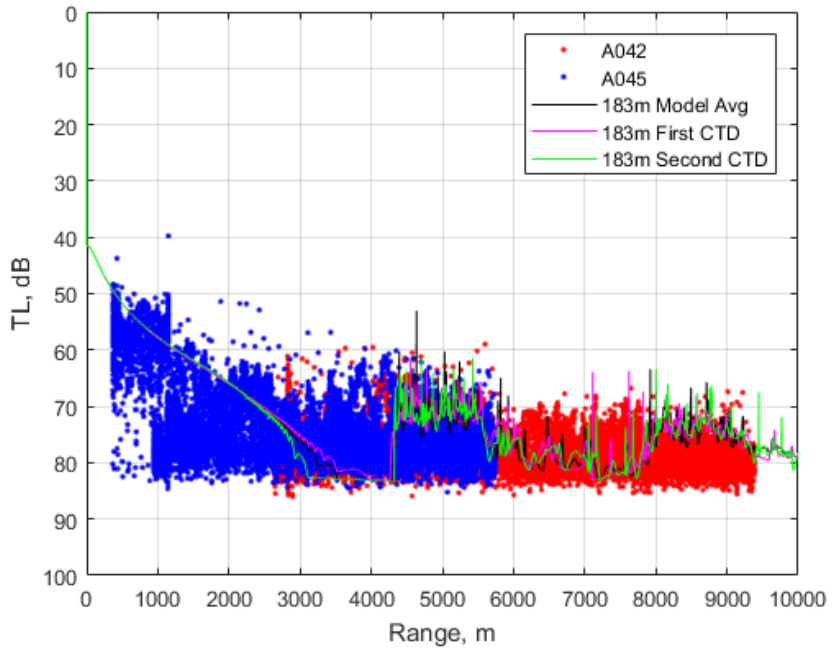

Figure 72. 45m Acousondes (A042, A045), EMATT at 183m, 2800 Hz

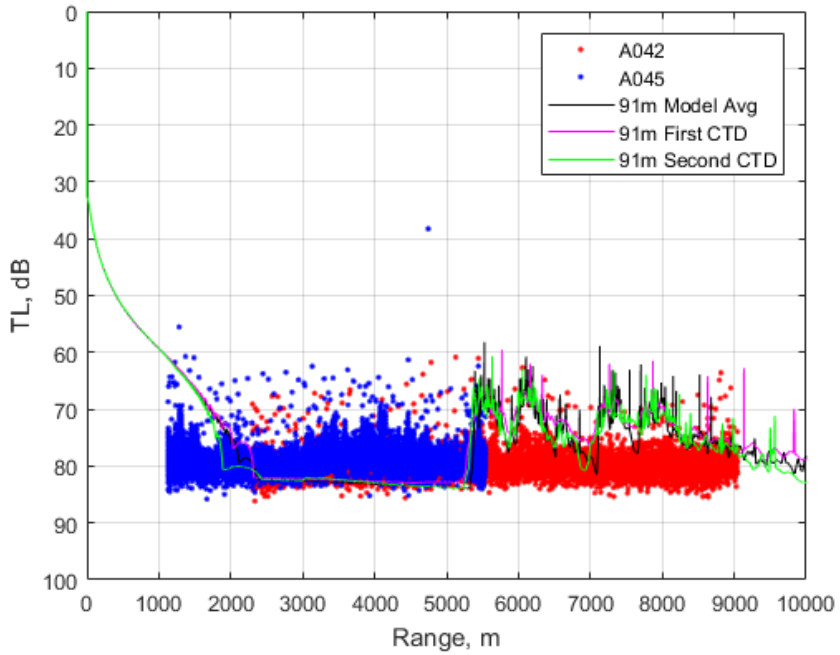

Figure 73. 45m Acousondes (A042, A045), EMATT at 91m, 2800 Hz

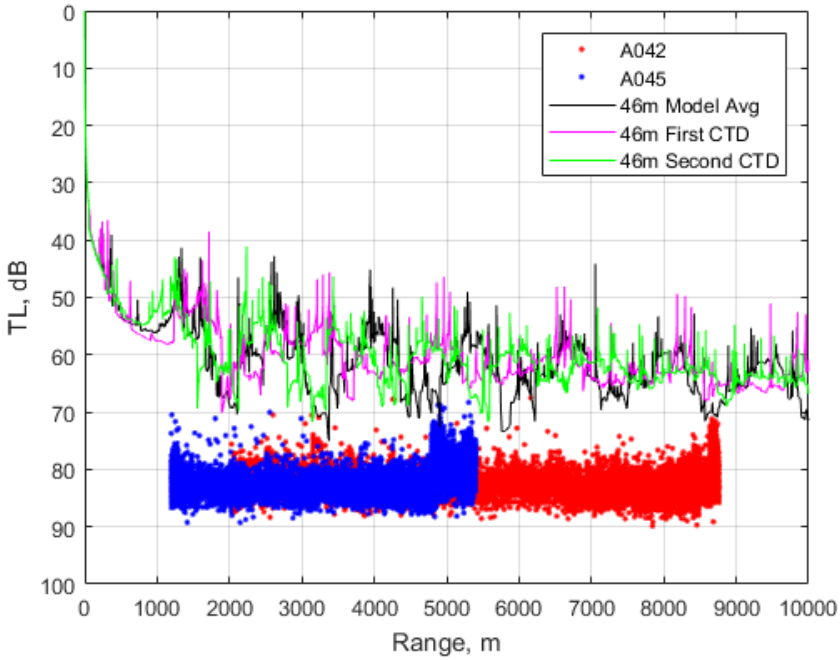

Figure 74. 45m Acousondes (A042, A045), EMATT at 46m, 2800 Hz

THIS PAGE INTENTIONALLY LEFT BLANK

LIST OF REFERENCES

Acoustimetrics, 2013: Acousonde 3A brochure. Accessed 26 July 2017. http://www.acousonde.com/downloads/Acousonde3A_Brochure.pdf

Bade, C., 2017: Study of integrated USV/UUV observation system performance in Monterey Bay. M.S. thesis, Dept. of Meteorology and Oceanography, Naval Postgraduate School, Monterey, California, *unpublished.*

Clark, B., 22 Jan 2015: The emerging era in undersea warfare. Center for Strategic and Budgetary Assessments, http://csbaonline.org/uploads/documents/CSBA6117-New-Era-Undersea-Warfare-Reportweb.pdf (Accessed 26 July 2017).

Dennis, B., and C. Mooney, 16 Aug 2016: A luxury cruise ship sets sail for the Arctic, thanks to climate change. *The Washington Post*, https://www.washingtonpost.com/news/energy-environment/wp/2016/08/16/a-luxury-cruise-ship-sets-sail-for-the-arctic-thanks-to-climate-change/ (Accessed 10 July 2017).

Hutt, D. L., 2012: An overview of Arctic Ocean acoustics. *AIP Conference Proceedings 1495*, Beijing, China, American Institute of Physics, 56-68, http://aip.scitation.org/doi/pdf/10.1063/1.4765907 (Accessed 22 July 2017).

Jackson, J. M., E. C. Carmack, F. A. McLaughlin, S. E. Allen, and R. G. Ingram, 2010: Identification, characterization, and change of the near-surface temperature maximum in the Canada Basin, 1993–2008, *J. Geophys. Res*., 115, C05021, doi:10.1029/2009JC005265.

Kapolka, D., 2016. Notes for PH3401 Introduction to sonar equations. Naval Postgraduate School, 262 pp.

Lockheed Martin, 2013: MK39 Expendable Mobile ASW Training Target and Field Programmability System (EMATT): A small, dynamic submarine-like target. Accessed 6 July 2017. http://www.lockheedmartin.com/content/dam/lockheed/data/ms2/documents/MK-39-productcard.pdf

Medwin, H., 2005: *Sounds in the sea: from ocean acoustics to acoustical oceanography*. Cambridge University Press, 643 pp.

Mellen, R.H. and H.W. Marsh, 1965: Underwater sound in the Arctic Ocean. AVCO Marine Electronics Office, 92 pp., http://www.dtic.mil/dtic/tr/fulltext/u2/718140.pdf (Accessed 31 July 2017).

Merklinger, H. M., and J. C. Osler, 2015: A few Canadian contributions to underwater acoustics. *Proc. Mtgs. Acoust. Volume 23*, Pittsburgh, PA, Acoustical Society of America, 1-20, http://asa.scitation.org/doi/pdf/10.1121/2.0000094 (Accessed 25 July 2017).

Minister of National Defence (MND), 2017: Strong, secure, engaged: Canada's defence policy. 113 pp. http://dgpaapp.forces.gc.ca/en/canada-defence-policy/index.asp (Accessed 5 July 2017).

National Oceanic and Atmospheric Administration (NOAA), 2017: Magnetic field calculators: Declination, https://www.ngdc.noaa.gov/geomag-web/#declination (Accessed 5 April 2017).

National Snow & Ice Data Center (NSIDC), 2017: Arctic sea ice maximum at record low for third straight year, http://nsidc.org/arcticseaicenews/2017/03/arctic-sea-ice-maximum-at-record-low/ (Accessed 3 July 2017).

National Snow & Ice Data Center (NSIDC), 2012: Arctic sea ice extent settles at record seasonal minimum, http://nsidc.org/arcticseaicenews/2012/09/arctic-sea-ice-extent-settles-at-record-seasonal-minimum/ (Accessed 3 July 2017).

Nelson, M. S, 2016: Short-range acoustic propagation under Arctic ice cover during ICEX-16. M.S. thesis, Dept. of Oceanography, Naval Postgraduate School, Monterey, California, 56 pp, https://calhoun.nps.edu/handle/10945/50603

Sevunts, L., 10 Feb 2017: U.S. Arctic strategy puts Canada and Russia on notice. Radio Canada International, http://www.rcinet.ca/en/2017/02/10/u-s-arctic-strategy-puts-canada-and-russia-on-notice/ (Accessed 10 July 2017).

Talley, L.D., G.L. Pickard, W.L. Emery and J.H. Swift (2011), *Descriptive physical oceanography: An introduction, 6th edition.* Elsevier Inc.

Urick, R. J., 1983: *Principles of underwater sound, 3rd edition*. McGraw-Hill, Inc.

INITIAL DISTRIBUTION LIST

1. Defense Technical Information Center
   Ft. Belvoir, Virginia

2. Dudley Knox Library
   Naval Postgraduate School
   Monterey, California